Microwave interaction in nonlinear metamaterials

Dissertation
zur Erlangung des Grades
eines Doktors der Naturwissenschaften

von

Mikhail Lapine
Moskau / Russland

genehmigt vom Fachbereich Physik der

UNIVERSITÄT OSNABRÜCK

Juli 2004

Contents

The work on this thesis was accompanied by following publications:

1. M. Gorkunov, M. Lapine, E. Shamonina, and K.H. Ringhofer, "Effective magnetic properties of a composite material with circular conductive elements", *European Physical Journal B*, **28**, 263–269 (2002).

2. M. Lapine, M. Gorkunov, and K.H. Ringhofer, "Nonlinearity of a metamaterial arising from diode insertions into resonant conductive elements", *Physical Review E*, **67**, 065601(R) (2003).

3. M. Gorkunov and M. Lapine, "Magnetically tunable metamaterial", *Proceedings of URSI EMTS 2004*, 388–390 (2004).

4. M. Lapine and M. Gorkunov, "Microwave interaction in nonlinear metamaterial", *Proceedings of URSI EMTS 2004*, 654–656 (2004).

5. M. Gorkunov and M. Lapine, "Tuning of nonlinear metamaterial band gap by external magnetic field", *submitted to Physical Review B* (2004).

6. M. Lapine and M. Gorkunov, "Three-wave coupling of microwaves in metamaterial with nonlinear resonant conductive elements", *submitted to Physical Review E* (2004).

Contributions to international conferences:

- M. Lapine, M. Gorkunov, E. Shamonina and K. H. Ringhofer, "Permeability of meta-material made of conductive rings", 9^{th} *International Conference on Electromagnetics of Complex Media*, (Bianisotropics-2002), Marrakech, Morocco (2002).

- E. Shamonina, L. Solymar, V. A. Kalinin, M. Lapine, K. H. Ringhofer, "Flux distribution in a non-resonant magnetic metamaterial", *Progress in Electromagnetics Research Symposium*, Cambridge, USA, (2002).

- M. Lapine, M. Gorkunov, E. Shamonina and K. H. Ringhofer, "Nonlinear Metamaterials Based on Resonant Conductive Elements", *Dielectrics for Emerging Technologies*, Edinburgh, Scotland, UK (2003).

- M. Gorkunov, M. Lapine, "Diode insertions make a tunable metamaterial", *Progress in Electromagnetic Research Symposium*, Pisa, Italy (2004).

- M. Lapine, M. Gorkunov, "Microwave interaction in metamaterial with nonlinear resonant conductive elements", *Progress in Electromagnetic Research Symposium*, Pisa, Italy (2004).

Chapter 1

Introduction

A few years ago a concept of metamaterial emerged, and since then metamaterials have been attracting an avalanche of research activity. To a great extent, this is stimulated by growing interest to the microwave range in electromagnetics. Rapid development of the microwave technology suggests elaboration of methods for efficient manipulations with microwaves. Metamaterials, being artificial structures, arranged as a lattice of identical elements or sets of elements, represent artificial crystals, designed for microwaves, and therefore, seem to be especially suitable for this purpose.

Theoretical investigations of artificial media, concerned with radiowave applications (Kalinin and Shtykov, 1991), or specific magnetic properties (e.g. Kostin and Shevchenko, 1993), date back to 80's and early 90's, although being neither widely known nor having drawn exciting conclusions.

Emerging of metamaterials concept and remarkable enhancement of research activity is associated with an idea to realize a medium with negative refraction index, put forward by Smith *et al.* (2000a). Theoretical analysis of media, possessing negative permittivity and permeability, was presented by Veselago (1968) long ago, but did not bring considerable impact at that time, due to lack of natural materials with negative permeability. Artificial structure elements with resonant magnetic behaviour, suggested by Pendry *et al.* (1999), opened a possibility to assemble metamaterials, having negative permeability in a certain frequency range, corresponding to microwaves (Pendry, 2001). In combination with components, which provide negative permittivity at the same range, a “Veselago”-medium can be constructed then (Smith *et al.*, 2000a; Tretyakov, 2001). Such metamaterials were successfully produced and used for experimental verification of negative refraction (Shelby *et al.*, 2001b; Grbic and Eleftheriades, 2002). One of the more contemporary and detailed reviews of the general features of a “Veselago”-media was given, e.g., by Lindell *et al.* (2001).

Obviously, the range of metamaterials application is not confined to the demonstration and use of the negative refraction phenomenon. For example, metamaterials were suggested for magnetoinductive waves guidance (Shamonina *et al.*, 2002a; Shamonina and Solymar, 2004). Furthermore, apparent analogy between metamaterials and crystals suggests that a number of methods, elaborated in optics, can be realized in metamaterials. The essentially larger scale, however, shifts the operating range of metamaterials to microwaves. An important advantage is that the properties of the whole metastructure can be controlled by adjusting the characteristics of individual elements and their arrangement — an option, not available for crystals.

In view of the above analogy, it is quite promising to provide nonlinearity to the response of structure elements, in order to afford numerous nonlinear phenomena, known in optics, to metamaterials. This idea is especially attractive due to the benefits of direct access to structure element properties. For instance, in 1991 Kalinin and Shtykov considered an artificial nonlinear medium of dipoles with diode inclusions, discussing arising electric nonlinear effects at radiowave frequencies. Accordingly, we proposed (Lapine *et al.*, 2003) to create a magnetic nonlinear metamaterial by inserting a nonlinear component into each structure element. The other paper (Zharov *et al.*, 2003), followed later that year, supposedly exploited the idea of Pendry *et al.* (1999) of enhancing nonlinear features of ordinary matter by subjecting latter to high fields, arising locally within the structure elements of metamaterial. From the phenomenological point of view, these ideas are essentially the same, as the nonlinear response in both cases is associated with particular components of each individual element.

Nowadays, most widely used structure elements are characterized with resonant magnetic properties. A typical example, suitable for experiments with three-dimensional metamaterials (Shelby *et al.*, 2001b; Bayindir *et al.*, 2002; Shelby *et al.*, 2001a), is a split ring resonator (Smith *et al.*, 2000a; Marqués *et al.*, 2002a) or its variations (Smith *et al.*, 2002; Marqués *et al.*, 2002b). Consequently, we consider a metamaterial, based on resonant conductive elements, which represent a generalization of various structure units. Provided with nonlinear components, such metamaterial can host immediate microwave interaction.

Despite the wide stream of publications, by the time the work on this thesis started, no adequate theory of the magnetic linear properties of metamaterial was given. Most of the attempts either are confined within studying the properties of a single element (Marqués *et al.*, 2002b, e.g.), a few elements (Gay-Balmaz and Martin, 2002), or reported physically inconsistent methods of performing macroscopic averaging (e.g. Pendry *et al.*, 1999; Smith *et al.*, 2000b; Ziolkowski, 2001).

Accordingly, we had to start with studying the linear properties of metamaterials, following the classical macroscopic approach (Landau and Lifschitz, 1984; Jackson, 1999). The developed theory (Chapter 2) confirmed that the linear magnetic properties of metamaterials demonstrate close analogy to electric properties of crystals.

Turning to nonlinear phenomena, at the first step (Chapter 3), we investigate the wave coupling, occurring in magnetically nonlinear metamaterial, for the limit of low amplitudes of the interacting waves. In this case a universal description of magnetic response, in terms of quadratic nonlinear susceptibility, is possible, offering a general model for various nonlinear processes.

For higher amplitudes, peculiarities of nonlinear insertions become essential, and the abovementioned universal description fails. Instead, a separate consideration is required, depending on particular nonlinear process as well as on the type of insertion. For the detailed analyzis, we focus on two nonlinear phenomena, having straightforward application potential: three-wave coupling of microwaves (Chapter 4) and tuning the band gap of metamaterial (Chapter 5). Nonlinear insertions can be generally divided into variable resistance and variable capacitance devices. Specific advantages and precautions, connected with employing both of them for performing the chosen nonlinear processes, are pointed out in respective chapters.

Keeping in mind growing experimental activity in the field of metamaterials, we give estimates for practical efficiency of each of the considered nonlinear effects, relying on the characteristics of available nonlinear components, and draw general recommendations for selecting them.

The concept of magnetically nonlinear metamaterial eventually appears to be quite fruitful, starting to attract wide scientific attention, as the recent emerge of publications from Agranovich *et al.* (2004) and Pendry (with O'Brien *et al.*, 2004) unambiguously show.

The main results and general conclusions of this work are summarized in Chapter 6, where the most promising directions of further research are also suggested.

Chapter 2

Linear properties of RCE-metamaterial

2.1 General remarks on macroscopic description

If the wavelength of electromagnetic waves inside the medium is much larger than both the element size and the distances between neighbouring elements, the properties of the metastructure with respect to such waves can be described with macroscopic permittivity and permeability. A typical size of metamaterial's "atom" (of the order of millimeters) satisfies this requirement for microwaves up to GHz-range. In general, the possibility to construct the medium from structural units possessing predetermined controllable properties provides a rare chance to study how effective macroscopic parameters of the substance are built up. This makes the whole field very interesting also from a general physical point of view, as one can apply here the well developed apparatus of the electrodynamics of condensed matter, expecting to obtain results which are quantitatively even more accurate than in the case of the optical theory where the structural units, i.e., atoms and molecules, are normally too complicated for a simple analytical treatment.

To derive the macroscopic features of the metamaterial from the known properties of the structural units and the periodic lattice parameters we develop a theory which has much in common with the theory of effective macroscopic dielectric response in crystals (Ryazanov, 1984, 1995; Gorkunov and Ryazanov, 1997). The general features of the latter can be summarized as:

- On the microscopic level mutual effects of the structural units are taken into account.

- The resulting microscopic non-locality is described by a characteristic length of response formation (local field formation length in local field theory). As a rule, it is of the order of several lattice constants.

- The effective response in the bulk area of the material can be considered as local if the wavelength of the electromagnetic wave is larger than the response formation length.

- Near material borders, a subsurface transition region appears with properties different from those in the volume. The characteristic thickness of the subsurface area is of the order of the response formation length.

In agreement with the macroscopic theory, the resonance frequency of the permeability is not determined solely by structure element characteristics, but depends markedly on the lattice parameters as well. This important fact was widely neglected in the main stream of publications due to the lack of appropriate consideration, as we discussed in the Introduction. Indeed, it is well known from optical response theory that the excitations in crystals are of collective nature and mutual interactions between atoms affect strongly the position of the resonance (Agranovich and Ginzburg, 1967). Therefore, there were sound reasons to expect that the same is true for metamaterials.

At frequencies above the material resonance, the permeability is negative. Performed analysis of the frequency dispersion of the permeability allows optimisation of the arrangement of the structural elements so that one can choose the most favourable lattice type and lattice constants to achieve, for example, a broader frequency range of the negative permeability.

Numerical simulation of the electromagnetic response of a finite sample of the metamaterial under the action of an external magnetic field proved completely the assumptions and results of the macroscopic approach. This fact does not only ensure the general principles but also allows us to expect that one can successfully use the numerical technique in cases when the structural units are not appropriate for analytical treatment. The most fruitful and, perhaps, the only possible way would be to solve numerically the field problem in a structure containing about thousand elements. Numerical averaging yields then the adequate macroscopic characteristics in a wide frequency range.

In this chapter we investigate the linear properties of a metamaterial, based on a simple structure unit, possessing non-trivial magnetic properties — a resonant conductive element (RCE).

RCE represents an element, which can be described with a resonant electric linear contour. If the dimensions of the contour are much smaller than the wavelength, then the current, magnetically induced in the contour, is the same along the contour line and the element can be characterized with effective resistance R, inductance L and capacitance C. The simplest example of such an element is a split conductive ring, for which contour parameters can be easily estimated theoretically (we consider this example in section 2.3). Note that various more complex elements, like split ring resonators (Pendry *et al.*, 1999; Shelby *et al.*, 2001a), also can be represented by effective contours, provided that the current cross-section is small enough compared to the element size (Shamonina *et al.*, 2002b; Marqués *et al.*, 2002b; Shamonin *et al.*, 2004). Should the effective contour parameters escape from analytical treatment, they can be easily determined experimentally by studying resonant properties of a single element (e.g. Gay-Balmaz and Martin, 2002). Accordingly, below we consider RCEs in general, turning to particular examples where necessary.

2.2 Averaging procedure and effective permeability

We suppose flat RCEs to be arranged so that the RCE planes are parallel and the elements form a kind of regular lattice. One should certainly keep in mind that the microscopic dimensions of the artificial substance are several orders of magnitude larger than those in crystals. The condition that the electromagnetic wavelength should be much larger than microscopic structural details is automatically fulfilled in crystals for the optical range. In the case of metamaterials, the analogous condition shifts the appropriate frequency range to microwaves with wavelengths of the order of several centimetres. Another difference, which is actually not so critical for the approach itself but appears during the interpretation of the results, is that we focus on how the RCEs affect magnetic field, while most effects in crystal optics are concerned with electric field. Due to the electric field — magnetic field symmetry of Maxwell's equations it is rather easy to find corresponding analogies between crystals and metamaterials. Nevertheless, the physical background is quite different.

As in the local response theory (Landau and Lifschitz, 1984; Ryazanov, 1984), we postulate that the response is formed at distances much smaller than the wavelength, i.e., we can neglect retardation while considering RCE interactions. This quasi-static limit allows us to separate magnetic effects from electric ones so that only the magnetic field affects the magnetization of the medium, defining the permeability. Electric fields are coupled by the polarization, define the permittivity and do not interfere with the magnetic properties at this stage. The resulting magnetic permeability is also not affected by the wavelength so that the latter can be treated as infinite. Then one can neglect the inhomogeneity of the magnetization and of the averaged fields and the problem is reduced to the behaviour of RCE arrays in the external homogeneous oscillating magnetic field.

Let all the RCEs lie in parallel planes normal to the z-axis. The structure is supposed to be infinite and the centres of the RCEs are located at the points $\mathbf{r}_n$. These points are assumed to form a regular spatial lattice so that each RCE has the same surrounding. We suppose the material of the structure elements to be non-magnetic so that the magnetization is only due to the currents induced in the RCEs. Though in general one should consider the full tensor of the permeability, from the chosen geometry it is obvious that the magnetization has only z-component, i.e., only μ_{zz} differs from unity. Therefore, only the z-component of the magnetic field is important, and the problem becomes scalar. Further we omit all appearing z and zz indices for the ease of notation.

Supposing the time dependence of fields and currents to have the oscillating form $e^{-i\omega t}$, one can write the electro-motive force $\mathcal{E}_n$ in the n-th RCE, induced by the external field $\mathcal{H}$, as

$$\mathcal{E}_n = i\omega\mu_0 S\mathcal{H}, \tag{2.1}$$

where S is an effective area of the RCE contour, which determines the magnetic flux via element. Using the multi-impedance matrix allows to write

$$\mathcal{E}_n = ZI_n + \sum_{n'\neq n} Z_{nn'}I_{n'}, \tag{2.2}$$

where I_n is the current induced in the n-th RCE, Z is the self-impedance and $Z_{nn'}$ is the mutual impedance between the RCEs n and n'.

The linear properties of each RCE are defined by the same self-impedance so that we can write

$$Z = -i\omega L + \frac{i}{\omega C} + R. \tag{2.3}$$

where we treat the self-inductance L, the capacitance C, and the resistance R, as predefined.

Obviously, due to the homogeneity of the external field and infinity of the medium, all the RCEs are in the same situation. Thus, all the currents $I_n = I$ are equal and the magnetic moment of each RCE equals to SI. The averaged media magnetization, defined as the magnetic moment density, is given by

$$M = \aleph SI, \tag{2.4}$$

where the volume concentration of RCEs, $\aleph$, is introduced. Combining Eqs. (2.1), (2.2), (2.4) together allows to obtain

$$\left(Z + \sum_{n' \neq n} Z_{nn'} \right) M = i\omega S^2 \aleph \mu_0 \mathcal{H}. \tag{2.5}$$

The total microscopic magnetic field (in the sense of being microscopic with respect to metamaterial properties) at the point $\mathbf{r}$ is given by the sum of the external field and the contribution of the RCEs:

$$H_{\text{mic}}(\mathbf{r}) = \mathcal{H} + \sum_n H_l(\mathbf{r} - \mathbf{r}_n), \tag{2.6}$$

where the function $H_l(\mathbf{r}')$ is defined as the value of the z-component of the magnetic field induced by the RCE, located at the coordinate origin, at the point $\mathbf{r}'$. According to the Biot-Savart's law $H_l(\mathbf{r}')$ can be presented as an integral along the RCE contour

$$H_l(\mathbf{r}') = \frac{I}{4\pi} \int \frac{[d\,\mathbf{l} \times (\mathbf{r}' - \mathbf{s})]_z}{|\mathbf{r}' - \mathbf{s}|^3}, \tag{2.7}$$

where the vector $\mathbf{s}$ is the radius vector of that point of the RCE, where $d\,\mathbf{l}$ is taken.

Since all the unit cells are identical, the field distribution is the same in all the cells. Therefore, the macroscopic averaging can be performed over the volume $V_m = \aleph^{-1}$ of one unit cell with any number m. The averaged value of the microscopic magnetic field (2.6) yields the macroscopic induction

$$B = \mu_0 \langle H_{\text{mic}} \rangle = \mu_0 \mathcal{H} + \frac{\mu_0}{V_m} \sum_n \int_{V_m} d\mathbf{r}\, H_l(\mathbf{r} - \mathbf{r}_n). \tag{2.8}$$

The radius vector $(\mathbf{r} - \mathbf{r}_n)$ passes all the cells with centres at $(\mathbf{r}_m - \mathbf{r}_n)$, where m takes all possible values. The summation over all n in (2.8) provides the result which is independent of the particular number m so that we can write

$$B = \mu_0 \mathcal{H} + \aleph \mu_0 \sum_{n'} \int_{V_{n'}} d\mathbf{r} H_l(\mathbf{r}) = \mu_0 \mathcal{H} + \aleph \mu_0 \int_V d\mathbf{r} H_l(\mathbf{r}). \tag{2.9}$$

The integration in the last term is to be performed over the large macroscopic volume V of the whole medium. We take the latter as the limit of a large sphere O, centered at the coordinate origin, with the radius r_s tending to infinity. Using the relation

$$\lim_{r_s \to \infty} \int_O d\mathbf{r} \frac{\mathbf{r}' - \mathbf{s}}{|\mathbf{r}' - \mathbf{s}|^3} = -\frac{4\pi}{3} \mathbf{s}, \tag{2.10}$$

it is easy to obtain

$$\int\limits_{O} d\mathbf{r} H_l(\mathbf{r}) = \frac{2}{3} S I = \frac{2}{3} \frac{M}{\aleph}, \tag{2.11}$$

which enables us to conclude that generally

$$B = \mu_0 \left(\mathcal{H} + \frac{2}{3} M \right). \tag{2.12}$$

The definitions $B = \mu_0 \mu H$ and $B = \mu_0 (H + M)$ allow us to express the effective permeability μ as

$$\mu = \frac{B}{B - \mu_0 M}. \tag{2.13}$$

Using Eqs. (2.5) and (2.12) allows to rewrite it as

$$\mu = \frac{Z + \sum\limits_{n' \neq n} Z_{nn'} + \frac{2}{3} i\omega S^2 \aleph \mu_0}{Z + \sum\limits_{n' \neq n} Z_{nn'} - \frac{1}{3} i\omega S^2 \aleph \mu_0}. \tag{2.14}$$

The mutual inductance of the RCEs in the limit of infinitely thin wire is given by the double integral along the RCE contours:

$$Z_{nn'} = i\omega \frac{\mu_0}{4\pi} \iint \frac{(d\,\mathbf{l}_n \cdot d\,\mathbf{l}_{n'})}{|\mathbf{s}_n - \mathbf{s}_{n'}|}. \tag{2.15}$$

Accordingly, the sum of the matrix elements in (2.14) can be represented as

$$\sum_{n' \neq n} Z_{nn'}(\omega) = -i\omega \mu_0 r \Sigma, \tag{2.16}$$

where r is some characteristic dimension of the RCE and Σ is a dimensionless parameter which depends only on the geometry of the RCE arrangement in the metastructure and can be calculated numerically.

For example, for two circular RCEs, having radii r_0, with the centres at points $\mathbf{r}_n$ and $\mathbf{r}_{n'}$ the integral (2.15) can be simplified as

$$Z_{nn'} = i\omega \mu_0 r_0 \Xi(\mathbf{r}_n - \mathbf{r}_{n'}) \tag{2.17}$$

with the dimensionless function

$$\Xi(\mathbf{r}) = \int\limits_0^{2\pi}\int\limits_0^{2\pi} \frac{r_0 \cos(\varphi_1 - \varphi_2) d\varphi_1 d\varphi_2}{4\pi \sqrt{\rho^2 + z^2 + 2r_0^2 \left(1 - \cos(\varphi_1 - \varphi_2)\right) + 2\rho r_0 (\cos\varphi_2 - \cos\varphi_1)}}, \tag{2.18}$$

where ρ, ϕ and z are the components of the vector $\mathbf{r}$ in cylindric coordinates; and then $\Sigma = \sum_{n' \neq n} \Xi(\mathbf{r}_n - \mathbf{r}_{n'})$.

Using form (2.16), we can rewrite the expression for the effective μ as

$$\mu = \frac{\dfrac{iZ}{\omega\mu_0 r} + \Sigma - \dfrac{2}{3}S^2 r^{-1}\aleph}{\dfrac{iZ}{\omega\mu_0 r} + \Sigma + \dfrac{1}{3}S^2 r^{-1}\aleph}. \tag{2.19}$$

One can see that the relation (2.19) is affected by the lattice order via the sum Σ only. This summation is performed over all the RCEs, i.e., over the macroscopic volume. This volume should be the same as for the averaging procedure, and we use the same spherical limit. Actually, it is necessary to perform the summation only over a finite and relatively small number of RCEs, which are located in the volume near the n-th one. Further increase in the radius r_s does not influence the summation result. For a good numerical accuracy of a few percent it is sufficient to set r_s to be only six times larger than the lattice constant. This satisfactory value of the distance r_s can be considered as a characteristic length of the local response L_{resp}. Although for different lattice types and various lattice constants L_{resp} differs in magnitude, it is, as a rule, of the order of several inter-element distances. The length L_{resp} is the parameter the wavelengths and sample dimensions should be compared with to make the macroscopic effective response approach valid.

2.3 Frequency dispersion of the permeability

The frequency dependence of the effective permeability given by (2.19) is controlled by the RCE self-impedance (2.3). For the illustrative analysis below we consider a thin circular RCE with radius r_0, made of wire with the radius r_w ($r_w \ll r_0$). The self-inductance of such an element equals (e.g. Landau and Lifschitz, 1984, chap. IV)

$$L = \mu_0 r_0 \left(\ln\frac{8r_0}{r_w} - 2\right) + \frac{\mu_0 r_0}{4}. \tag{2.20}$$

For a given inductance, we choose the value of the implemented capacitance C which is necessary to ensure desirable resonance frequency of a single RCE. To be consistent with the available experimental information (Smith *et al.*, 2000a), we set the latter equal to 3 GHz. The corresponding value of the cyclic resonance frequency of a single RCE,

$$\omega_0 = \frac{1}{\sqrt{LC}}, \tag{2.21}$$

equals $6\pi \cdot 10^9$ rad/s. Appropriate capacitance value could be obtained, for instance, by a small slit in the RCE contour, so that

$$C = \varepsilon_0 \pi r_w^2 \iota^{-1},$$

where the slit width ι should be of the order of microns for the RCE radius $r_0 = 2$ mm and wire radius $r_w = 0.1$ mm. Actually, one can make capacitance plates larger than the wire cross section which will allow to increase the slit width.

To estimate the resistive losses in the wire one should take skin effect into account, as the frequencies are rather high. The skin depth in a material with the characteristic conductivity of copper ($\sigma = 0.65 \cdot 10^8$ S/m),

$$\delta = \left(\frac{1}{2}\sigma\omega\mu_0\right)^{-1/2}, \tag{2.22}$$

appears to be several orders of magnitude smaller than the wire radius. Thus only thin subsurface layer of the wire is really active, and the resistance equals

$$R = r_0(\sigma l \delta)^{-1}. \tag{2.23}$$

The corresponding quality factor of the RCE is then of the order of thousand, which is in good agreement with the experimental data (Smith *et al.*, 2000a; Shelby *et al.*, 2001a). We use the physical parameters mentioned above for the illustrative calculations described below.

For the analysis of frequency dispersion, it is convenient to present the effective permeability (2.19) in the general resonance form:

$$\mu(\omega) = 1 - \frac{A\omega^2}{\omega^2 - \omega_r^2 + i\Gamma\omega}, \tag{2.24}$$

with the resonance amplitude

$$A = \mu_0 S^2 \aleph L^{-1} \frac{\omega_r^2}{\omega_0^2}, \tag{2.25}$$

resonance width

$$\Gamma = R L^{-1} \frac{\omega_r^2}{\omega_0^2}, \tag{2.26}$$

and the resonance frequency of the medium,

$$\omega_r = \omega_0 \left(1 + \mu_0 r \Sigma L^{-1} + \frac{1}{3}\mu_0 S^2 \aleph L^{-1}\right)^{-1/2} = \omega_0 \left(\frac{L_\Sigma}{L} + \frac{1}{3}\frac{\mu_0 \aleph S^2}{L}\right)^{-1/2}, \tag{2.27}$$

where we introduced a combined mutual and self-inductance $L_\Sigma = L + \mu_0 r \Sigma$, using relation (2.16).

Relation (2.27) demonstrates that the resonance of the medium can be remarkably shifted from the single RCE resonance due to the mutual interaction. This shift increases as the volume concentration of RCEs is increased. The exact values appear to depend, via the sum Σ, on the type of the regular spatial ordering. The lattices, reported in literature (e.g. Pendry *et al.*, 1999; Shelby *et al.*, 2001b), are of the layered type. It appears to be technically simpler to pack first the RCEs in some regular order on flat surfaces and afterwards place these planes in a regular pattern to form the sample. With this technique, the simplest case seems to be a tetragonal lattice, where the RCEs form a square structure in the planes and all the planes are put just one above another so that columns of RCEs are formed. A view from the top of the medium is shown in Fig. 2.1 (a). Packing within a plane can have another symmetry: the hexagonal one is shown in Fig. 2.1 (b). It is also possible to shift the RCEs in neighbouring layers with respect to each other. We call this a "shifted lattice". The shift is the most effective when the centre of a RCE is located equidistantly from the RCE centres in the nearest layer. Such shifted tetragonal and hexagonal lattices are shown in Fig. 2.1 (c) and (d), respectively (two neighbouring layers are shown).

Obviously, to enhance the mutual effects one should increase the volume

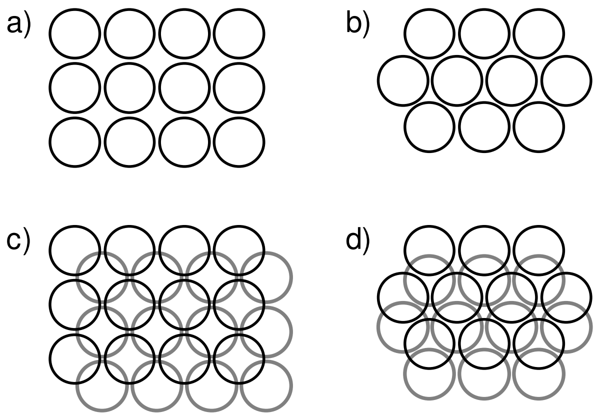

Figure 2.1: Four types of studied lattices. Tetragonal (a), hexagonal (b), shifted tetragonal (c) and shifted hexagonal (d) lattices are shown as seen from the top of the multi-layered structure. In (c) and (d) cases two neighbouring layers are shown in different hue (black and grey circles, respectively).

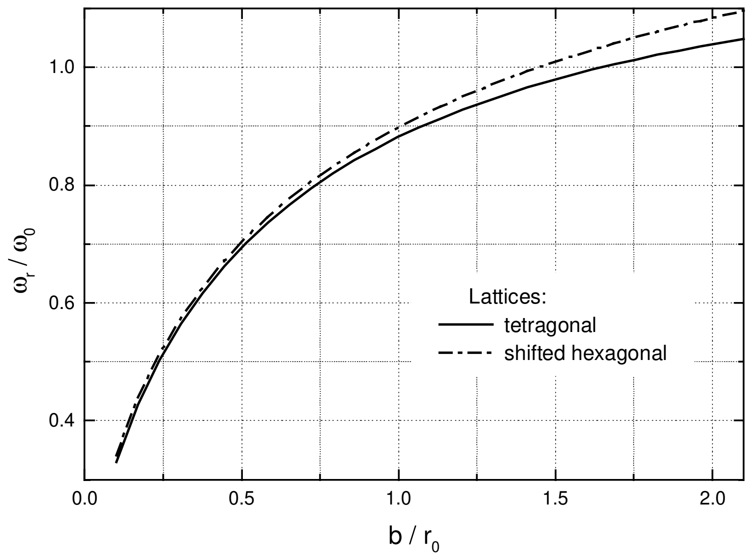

Figure 2.2: Relative resonance frequency shift as a function of the ratio of the interlayer distance to the RCE radius.

concentration of RCEs. The distance a between the RCE centres within a plane is limited by two RCE radii; below we accept $a = 2.1\, r_0$. The interlayer distance b could be technically limited, we assume the value $b = 0.1\, r_0$ to be achievable.

The calculated resonance frequency dependencies on the lattice constant b for different lattices are shown in Fig. 2.2. They depend only slightly on the lattice type, and we show the two most deviating curves, for tetragonal and shifted hexagonal arrangements. It is clear that one can drastically decrease the resonance frequency increasing packing density of the conductive elements.

At frequencies larger than ω_r the real part of the permeability (2.24) is negative. It grows with further increase in frequency and becomes positive at a frequency $\tilde{\omega}$, which can be found from the condition $\mu(\tilde{\omega}) = 0$. To use the metamaterial for the demonstration of the negative refraction phenomenon, it is preferable to have a broader frequency range of negative permeability. It is convenient to measure this broadness by the ratio

$$\Delta = \frac{\tilde{\omega}^2 - \omega_r^2}{\omega_r^2}, \tag{2.28}$$

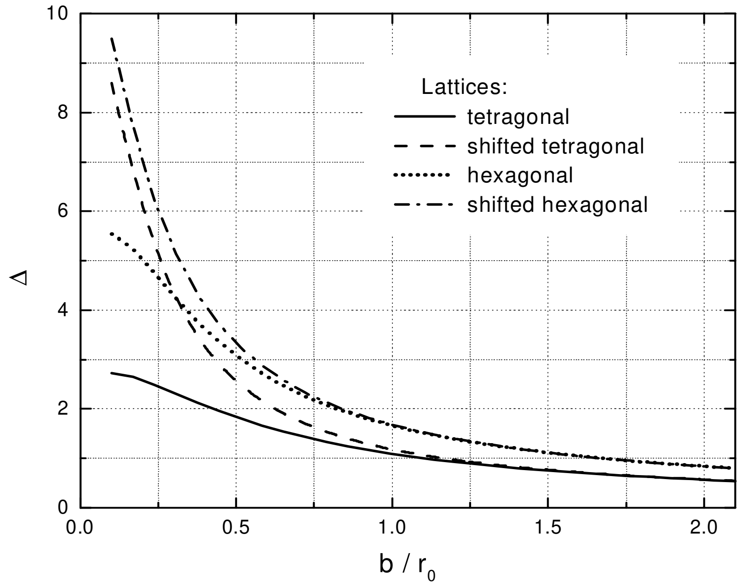

Figure 2.3: Relative broadness Δ of the negative permeability frequency range as a function of the ratio of the interlayer distance b to the RCE radius r_0.

which is, according to Eq. (2.24),

$$\Delta = \frac{\mu_0 S^2 \aleph L^{-1}}{1 + \mu_0 r \Sigma L^{-1} - \frac{2}{3}\mu_0 S^2 \aleph L^{-1}}. \tag{2.29}$$

The calculated dependency of this expression on the lattice constant b for different lattices is shown in Fig. 2.3. The general tendency for all lattices is the significant broadening of the negative permeability range as the volume concentration of RCEs increases. It can be clearly seen that the hexagonal order within a plane provides considerably wider broadening than the square one. Shifting of neighbouring layers is very profitable at small values of b. As a result, we can conclude that the shifted hexagonal order is the most appropriate. It provides an up to three times broader frequency range compared with the tetragonal lattice used in (Shelby *et al.*, 2001b).

To explain the importance of the lattice type for the value Δ it is useful to notice that with decrease in b both the lattice sum Σ and the concentration $\aleph$ increase markedly. In the denominator of Eq. (2.29) the corresponding last two terms partially compensate each other. Therefore, the difference in the lattice sums for different lattices at a given density, which is not so crucial for the resonance position, plays an important role here. The smaller is Σ, the larger is Δ. The contribution to the sum coming from different RCEs may have the opposite signs: the largest positive terms arise from the RCEs just one above another in neighbouring layers, while contribution from the neighbouring RCEs within the same layer provide the largest negative terms. Therefore, Δ is smallest in the case of tetragonal lattice — there are only 4 neighbouring RCEs within the same layer, while the influence of the inter-layer RCEs is great. The hexagonal lattice provides 6 in-layer neighbours and also a higher RCE concentration $\aleph$. In the shifted lattices positive inter-layer terms are reduced, especially for the small b, when the strong influence of adjacent vertical neighbours (one exactly above another) is eliminated. This makes clear why the shifted hexagonal lattice gives the broadest negative permeability region.

2.4 Numerical simulation of the finite metamaterial

The circular conductive elements provide a rare opportunity to obtain the analytical expression for the effective response of the metamaterial. Nevertheless, there is a number of interesting structural units which could be treated only numerically. In a numerical simulation of a metamaterial behaviour one can deal only with a finite sample and it is worthwhile from the computational point of view to minimize the number of structural units, yet keeping in mind that the macroscopic approach must be still valid. Below we determine numerically the macroscopic parameters of the RCE metamaterial. This allows us to illustrate the postulates and principles of the macroscopic approach and to check the results obtained above. On the other hand, this comparison allows to optimise the numerical method itself, as one can determine the proper operating range of the method, the minimal sufficient size of the metamaterial, etc.

We study a rectangular sample of the metamaterial under the action of a homogeneous external magnetic field which acts along the z-direction, normal to the RCE planes. The currents induced in different RCEs are now different and can be found with the help of the multi-impedance matrix equation

$$\sum_{n'} Z_{nn'} I_{n'} = i\omega\mu_0 S\mathcal{H}. \tag{2.30}$$

where all the diagonal terms of the impedance matrix are the same and equal to the self-impedance (2.3), while the non-diagonal ones are given by Eqs. (2.17–2.18). Calculating and inverting the $Z_{nn'}$ matrix, we can get the currents in each RCE numerically.

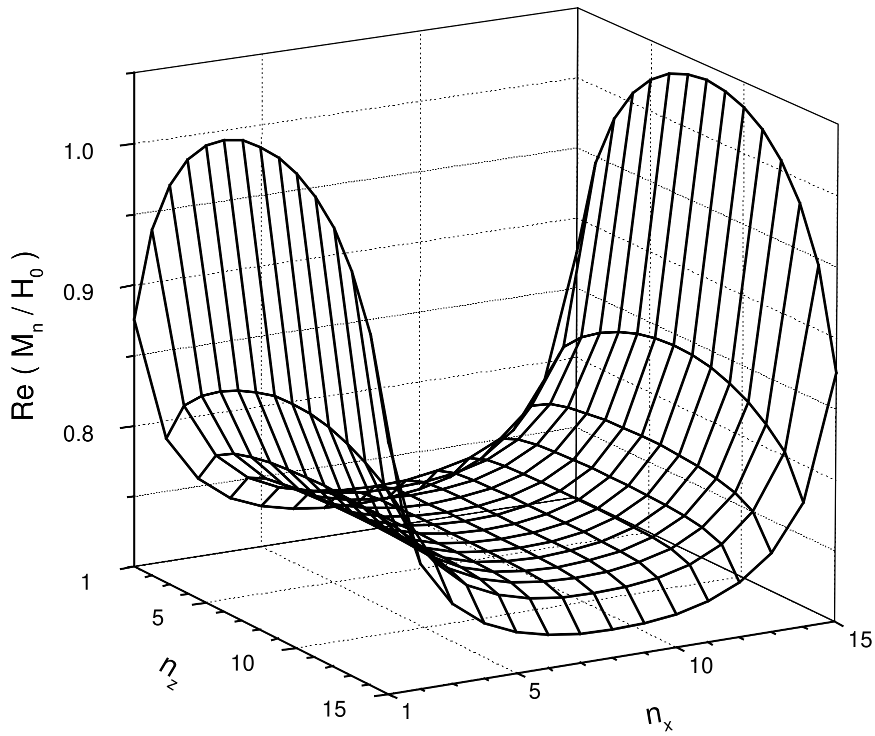

Figure 2.4: Numerically calculated normalised magnetization distribution in the sample consisting of $15 \times 15 \times 15$ RCEs.

To demonstrate a typical current distribution inside the material we show the magnetization pattern inside the sample consisting of $15 \times 15 \times 15$ circular RCEs (Fig. 2.4). Calculations were made for the tetragonal lattice with $a = 2.1\, r_0$ and $b = 0.5\, r_0$, i.e., for the structure with remarkable mutual effects, at the frequency $0.6\, \omega_0$. The position of a RCE is characterized by three numbers (n_x, n_y, n_z) taking values from 1 to 15. We show the distribution in a plane in the middle, $n_y = 8$. The magnetization (2.4) is determined for each RCE with $I = I_n$, and normalized to $\mathcal{H}$. The imaginary part is three orders of magnitude smaller than the real one and is not shown. It can be clearly seen that there is a noticeable flat region in the central area where the magnetization is almost homogeneous. Close to the borders, subsurface areas with specific properties appear. The characteristic thickness of these perturbed layers is about several lattice constants, confirming the idea of the local response formation within such a length.

The current distribution allows us to calculate the microscopic magnetic field according to Eq. (2.6). We assume the central unit cell in the sample to be the most representative for the bulk; then the averaging procedure (2.8) can be carried out by numerical integration over this unit cell. Using the value of the magnetization (2.4) in this cell, we get finally the permeability value according to Eq. (2.13). The effective permeability obtained in this way appears to be independent of the shape of the sample; the only necessary condition is that the sample dimensions should be larger than the response formation length. For instance, the results of the numerical simulation are the same for the samples of $11 \times 11 \times 31$ and $19 \times 19 \times 11$ RCEs. Actually, the accuracy of about one percent could be achieved already by using a sample having 11 RCEs in each dimension.

The comparison of the numerically obtained permeability as a function of frequency with the analytical formula (2.24) is shown in Fig. 2.5. The current distribution remains similar to Fig. 2.4 within the whole frequency range except for the two narrow regions $\omega = (0.700 \pm 0.002)\,\omega_0$ in the close vicinity of the resonance and $\omega = (1.2 \pm 0.2)\,\omega_0$ around the frequency at which the permeability is zero. Inside these regions a periodic modulation of the currents appears, with the period of the modulation being of the order of a few lattice constants. This inhomogeneity results from the excitation of standing exciton waves with extremely large wave vectors. Such waves are

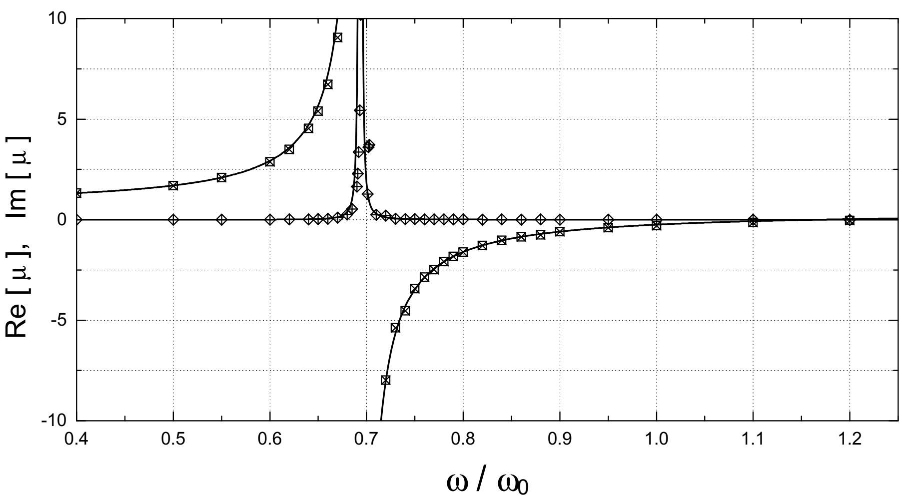

Figure 2.5: Frequency dispersion of the permeability, obtained numerically (squares for the real and diamonds for the imaginary part), compared with the analytical formula (solid line, real part; dashed line, imaginary part). Calculations were made for the tetragonal lattice with $a = 2.1\,r_0$, $b = 0.5\,r_0$.

well known in optics (Agranovich and Ginzburg, 1967). Due to their small wavelength, they arise in theory even if retardation is neglected, being called Coulomb-type excitons. Analogous phenomena in metamaterials are connected with an emerging concept of magnetoinductive waves, put forward by Shamonina *et al.* (2001), and currently thoroughly investigated (Shamonina *et al.*, 2002a; Shamonina and Solymar, 2004; Wiltshire *et al.*, 2004).

The short-range inhomogeneity of the current distribution at frequencies mentioned above makes the response there non-local. Corresponding numerical values of the permeability are physically meaningless in these narrow frequency intervals. We omit them in the resulting curve in Fig. 2.5. In all the remaining frequency range one can observe excellent agreement between analytical and numerical results for the real part of the permeability. Extremely steep behaviour of the imaginary part near the resonance leads to the large sensitivity of the result to the errors of the numerical calculations. Nevertheless, we can report that the resonance frequency was determined numerically with an error of less than one percent.

This analysis allows us to consider such numerical calculations to be a very promising way to predict the metamaterial response in the case of more complicated structural units.

2.5 Discussion

In this chapter we demonstrated the capability of the macroscopic approach to describe successfully the properties of a metamaterial constructed of circular conductive elements. The method of calculating an effective magnetic response can be easily generalized for more complicated structural units and various types of their ordering in metamaterials. For instance, it allows generalization for a 3D lattice where the planes of conductive elements are arranged in three perpendicular directions, as suggested by Pendry *et al.* (1999). For the cases when the unit cell is too complicated for an analytical consideration, the suggested numerical method is nevertheless applicable. We have shown that for a very precise *ab initio* permeability calculation it is necessary to be capable of studying numerically a system of about thousand structural units.

We believe that further application of the ideas well developed in the optical theory would be extremely helpful in the new intensively growing field of metamaterials. It appears that a number of ideas and concepts, which have been approved in optics, are easily applicable to this case. For example, one can notice that the structure of the expression (2.19) for the permeability has very much in common with the permittivity of uniaxial crystals, obtained in terms of the optical local field theory (Gorkunov and Ryazanov, 1997). Moreover, taking the limit of low RCE concentration and assuming the lattice to be cubic, one can show Σ to be equal to zero due to symmetry, which leads to the relation

$$\frac{\mu - 1}{\mu + 2} = \frac{1}{3}\aleph\frac{\omega\mu_0 S^2}{iZ}. \tag{2.31}$$

This shows a direct analogy to the Clausius-Mossotti relation for the permittivity of an isotropic substance with point polarizable particles. The product $-i\omega\mu_0 S^2 Z^{-1}$ plays here the role of the magnetic polarizability of a single structural unit.

Chapter 3

Nonlinear magnetic susceptibility

3.1 Anticipating nonlinearity

In the previous chapter we have presented a linear theory of the magnetic response for a metastructure assembled as a regular lattice of RCEs. We pointed out that the linear properties of metamaterials demonstrate close analogy to those of crystals. As it was already mentioned, in view of this analogy, metamaterials are likely to host direct microwave interaction, when the response of the structure elements is nonlinear. Following the idea of Kalinin and Shtykov (1991), in order to provide nonlinearity to the metamaterial we are concerned with, we introduce a nonlinear insertion to each RCE.

In this chapter we consider the case of low amplitudes of the propagating waves and show, how the nonlinear voltage-current characteristic of the insertion provides nonlinearity to the response of the metamaterial in the limit of low nonlinearity. The arising multi-wave interactions allow to affect the wave propagation directly in a convenient "optical" manner, i.e., without conversion into electronic signals. We find that the resulting macroscopic susceptibility depends not only on the single element's susceptibility, but also contains renormalization factors determined by the linear response of the material at the frequencies of the interacting waves.

3.2 RCE with a nonlinear insertion

Considering nonlinear coupling in the metamaterial, we are interested in the relationship between the magnetization of metamaterial and the macroscopic magnetic fields inside it, at all the frequencies involved. We have seen that magnetization is determined by the currents, induced in RCEs by the fields of propagating waves. Should the response of RCE be nonlinear, a coupling between these currents arises. Obviously, the mutual interaction of elements remains linear and is not relevant at this stage. Consequently, in the metamaterial of RCEs with nonlinear insertions, wave coupling is provided on the level of structure elements. Thus we are first looking for the relationship between currents and voltages, induced at all the interacting frequencies, analyzing a single element, subjected to oscillating magnetic field.

The DC current-voltage characteristic of an insertion at low voltages can be approximated by

$$I = \frac{1}{\mathcal{R}_0}(U + \gamma U^2), \tag{3.1}$$

where I is the current through the insertion to which the voltage U is applied, $\mathcal{R}_0$ is the ohmic resistance of insertion, and γ is a parameter standing for the nonlinearity. Here the voltage should be much smaller than $\tilde{U} \sim 1/\gamma$.

In the AC case, it is necessary to account for frequency dispersion, which is easier to do if one deals with Fourier components. Accordingly, we substitute all the time dependencies by sums of monochromatic components, so that, e.g., the time dependence of the current is $I(t) = \sum_\vartheta I(\omega_\vartheta)e^{-i\omega_\vartheta t} \quad \vartheta = \pm 1, \pm 2, \ldots$, where we use the notation with $\omega_{-\vartheta} \equiv -\omega_\vartheta$, $I(\omega_{-\vartheta}) \equiv I^*(\omega_\vartheta)$, which includes automatically the complex conjugates.

Due to the nonlinear term in (3.1), Fourier components at combinational frequencies will be coupled. Keeping up to bilinear in I terms, we can represent the voltage-current characteristic as the following:

$$\begin{aligned} U(\omega_\vartheta) = {} & \mathcal{Z}(\omega_\vartheta)I(\omega_\vartheta) + \\ & \frac{1}{2}\sum_\eta \gamma(\omega_\vartheta; \omega_\eta, \omega_\vartheta - \omega_\eta) \times \mathcal{Z}(\omega_\vartheta - \omega_\eta)\mathcal{Z}(\omega_\eta)I(\omega_\vartheta - \omega_\eta)I(\omega_\eta), \end{aligned} \tag{3.2}$$

where $\gamma(\omega_\vartheta; \omega_\eta, \omega_\vartheta - \omega_\eta)$ is generally complex and $\mathcal{Z}(\omega)$ is the linear impedance of the insertion, i.e., $\mathcal{Z} \to \mathcal{R}_0$ at $\omega \to 0$.

When the insertion is implemented into the RCE, the response of the whole element depends on the particular position and connections. However, for a reasonable arrangement, the element with insertion can be still described by effective contour. If the nonlinearity is low, the current in the RCE with insertion under the action of external e.m.f. is determined by

$$\big(Z(\omega) + \mathcal{Z}(\omega)\big)I(\omega) + U^{(2)}(\omega) = \mathcal{E}(\omega), \quad \text{with} \tag{3.3}$$

$$U^{(2)}(\omega) = \frac{1}{2}\sum_\eta \zeta(\omega_\vartheta; \omega_\eta, \omega_\vartheta - \omega_\eta)I(\omega_\vartheta - \omega_\eta)I(\omega_\eta), \tag{3.4}$$

where $U^{(2)}$ is the nonlinear part of the response. Here the nonlinear properties of insertion are described with the parameter ζ, which generally depends on the insertion characteristics (γ and $\mathcal{Z}$) as well as on the way of inserting. For example, if the insertion is implemented in-series into a split conductive ring,

$$\zeta(\omega_\vartheta;\omega_\eta,\omega_\upsilon) = \gamma(\omega_\vartheta;\omega_\eta,\omega_\upsilon)\mathcal{Z}(\omega_\upsilon)\mathcal{Z}(\omega_\eta). \tag{3.5}$$

Now we are ready with the single RCE's response.

3.3 Quadratic magnetic susceptibility

Turning to analysis of the whole metamaterial, we follow the macroscopic approach, developed in the previous chapter. In order to take the insertions into account, we extend the impedance equation (2.2) in accordance with Eq. (3.3), arriving at system

$$\big(Z(\omega) + \mathcal{Z}(\omega)\big)I_n(\omega) + \sum_{n'\neq n} Z_{nn'}(\omega)I_{n'}(\omega) + U_n^{(2)}(\omega) = \mathcal{E}_n(\omega), \tag{3.6}$$

where $\mathcal{E}_n(\omega)$, the same for all the elements, is given by (2.1):

$$\mathcal{E}(\omega) = i\mu_0 S\omega\mathcal{H}(\omega). \tag{3.7}$$

We remind that in the homogeneous metamaterial all the currents, induced by e.m.f. (3.7), are equal, and so system (3.6) is reduced to the equation

$$\Big[Z(\omega) + \mathcal{Z}(\omega) + \sum_{n'\neq n} Z_{nn'}(\omega)\Big]I(\omega) + U^{(2)}(\omega) = \mathcal{E}(\omega). \tag{3.8}$$

For the ease of notation, we combine all the impedances involved, into

$$Z_\Sigma(\omega) = Z(\omega) + \mathcal{Z}(\omega) + \sum_{n'\neq n} Z_{nn'}(\omega). \tag{3.9}$$

Rewriting (3.8) for multiple frequencies, with the help of (3.4) we obtain a system

$$Z_\Sigma(\omega_\vartheta)I(\omega_\vartheta) = \mathcal{E}(\omega_\vartheta) + \frac{1}{2}\sum_\eta \zeta(\omega_\vartheta;\omega_\eta,\omega_\vartheta-\omega_\eta)I(\omega_\vartheta-\omega_\eta)I(\omega_\eta). \tag{3.10}$$

The system (3.10) shows that the current component at each frequency is determined not only by the e.m.f. at that frequency, but also by the current components induced at two other frequencies, so that a three-wave interaction occurs. Accordingly, we consider below ω_1, ω_2 and ω_3, such that $\omega_1+\omega_2=\omega_3$. Then from (3.10) we get for the current induced at ω_3

$$Z_\Sigma(\omega_3)I(\omega_3)=\mathcal{E}(\omega_3)+\zeta(\omega_3;\omega_1,\omega_2)I(\omega_1)I(\omega_2). \tag{3.11}$$

For the linear in ζ approximation we can substitute $I(\omega_2)$ and $I(\omega_1)$ in the right-hand side of (3.11) for the expressions, obtained from (3.10) written for ω_1, ω_2, neglecting the terms with ζ. Then we can express $I(\omega_3)$ via $\mathcal{E}(\omega_1)$, $\mathcal{E}(\omega_2)$ and $\mathcal{E}(\omega_3)$. In turn, this allows to obtain an equation for the magnetization at ω_3:

$$M(\omega_3)=\frac{i\aleph\mu_0S^2\omega_3}{Z_\Sigma(\omega_3)}\mathcal{H}(\omega_3)-\frac{\zeta(\omega_3;\omega_1,\omega_2)\aleph\mu_0^2S^3\omega_1\omega_2}{Z_\Sigma(\omega_3)Z_\Sigma(\omega_2)Z_\Sigma(\omega_1)}\mathcal{H}(\omega_1)\mathcal{H}(\omega_2), \tag{3.12}$$

where we used relations (2.4) and (3.7).

As it was shown in previous chapter (see (2.12), p. 9), $B=\mu_0\left(\mathcal{H}+\frac{2}{3}M\right)$ notwithstanding the structure element's peculiarities. With the general definition $B=\mu_0(H+M)$, we can express

$$\mathcal{H}=H+\frac{1}{3}M. \tag{3.13}$$

Using this relation, we can solve (3.12) for $M(\omega_3)$. In the linear approximation we obtain $M(\omega_3)=\chi_{\mathsf{M}}(\omega_3)H(\omega_3)$, where the factor

$$\chi_{\mathsf{M}}(\omega)=\frac{\mu_0\aleph S^2\omega}{-\frac{1}{3}\mu_0\aleph S^2\omega-iZ_\Sigma(\omega)}. \tag{3.14}$$

stands for the linear part of the magnetic susceptibility. The corresponding permeability $\mu(\omega)=1+\chi_{\mathsf{M}}(\omega)$, upon algebraic conversion, coincide with (2.19). Consequently, $\chi_{\mathsf{M}}(\omega)$ shows resonance behaviour with the resonance frequency (2.27).

Returning to the 1-st order nonlinear consideration and keeping the terms linear in ζ, we express finally $M(\omega_3)$ in a form which is analogous to the polarization of a medium with quadratic dielectric nonlinearity:

$$M(\omega_3)=\chi_{\mathsf{M}}(\omega_3)H(\omega_3)+\chi_{\mathsf{M}}^{(2)}(\omega_3;\omega_1,\omega_2)H(\omega_1)H(\omega_2) \tag{3.15}$$

with the quadratic nonlinear susceptibility

$$\chi_{\mathsf{M}}^{(2)}(\omega_3;\omega_1,\omega_2)=\frac{\zeta(\omega_3;\omega_1,\omega_2)}{i\mu_0S^3\omega_3}\,\aleph^{-2}\chi_{\mathsf{M}}(\omega_1)\chi_{\mathsf{M}}(\omega_2)\chi_{\mathsf{M}}(\omega_3). \tag{3.16}$$

Therefore, in spite of the completely different physical background, one can deal with the nonlinear interaction of electromagnetic waves in the proposed metamaterial using the well developed apparatus of the nonlinear optics. The general symmetry of Maxwell equations with respect to the magnetic field — electric field transposition allows to expect that the whole variety of known nonlinear optical processes can have corresponding analogues in metamaterials.

Analyzing the structure of (3.16), it is easy to notice that the first factor is completely determined by the single element properties. Its multiplication with the linear susceptibilities taken at the frequencies of interacting waves performs a kind of renormalization and can be treated as the result of the influence of the surroundings. This kind of renormalization appears, for instance, in the derivation of nonlinear dielectric susceptibility in optical materials (Bloembergen, 1965; Schubert and Wilhelmi, 1971). Like the optical nonlinearity, the nonlinearity of the magnetic metamaterial increases resonantly as one of the frequencies involved approaches the resonance of the linear susceptibility.

3.4 Practical estimates for low nonlinearity

To estimate the macroscopic characteristics of the nonlinear metamaterial of the presented type, we consider an example of metastructure based on split rings with radius $r_0 = 2\,\mathrm{mm}$ and wire diameter $r_w = 0.1\,\mathrm{mm}$, arranged with the density $\aleph \sim r_0^{-3}$. Among numerous diode types, backward diodes were reported to possess the best sensitivity and the highest nonlinearity (Sze, 1981; Schulman *et al.*, 2001). Such a diode insertion, having a cross-section, similar to the wire, is characterized (Schulman *et al.*, 2001) by $\gamma \approx 30\,V^{-1}$ and $\mathcal{Z} \approx \mathcal{R}_0 \approx 10\,\Omega$. Although diodes might allow for higher nonlinearity, equation (3.2) is valid only under the assumption that the nonlinear contribution is much smaller than the linear one. They become comparable when the current reaches characteristic value $\tilde{I}(\omega) \sim \left(|\gamma \mathcal{Z}(\omega)|\right)^{-1}$, which corresponds to the magnetization $\tilde{M}(\omega) = nS\tilde{I}(\omega)$. Accordingly, the magnetic field in the metamaterial must be much lower than $\tilde{H}(\omega) = \tilde{M}(\omega)/\chi_{\mathsf{M}}(\omega)$. Assuming that the pump frequency is ω_1, and $H(\omega_1) \sim 0.1\tilde{H}(\omega_1)$, using (3.5), we can estimate the maximal amplitude of the nonlinear modulation of the magnetic susceptibility as

$$\chi_{\mathsf{M}}^{(2)}(\omega_2;\omega_0,\omega_1)H(\omega_1) \sim 0.1\frac{\mathcal{Z}(\omega_2)}{\mu_0 \aleph S^2 \omega_3}\chi_{\mathsf{M}}(\omega_1)\chi_{\mathsf{M}}(\omega_2). \tag{3.17}$$

For frequencies not close to the resonance, we can assume $\chi_{\mathsf{M}}(\omega_1)\chi_{\mathsf{M}}(\omega_2) \sim 1$, which provides a noticeable nonlinear contribution of the order of 0.001 with the pump field limited by about 0.1 A/m.

The nonlinearity can be further enhanced by either decreasing the diode cross-section (that raises $\mathcal{Z}$), or choosing the frequencies closer to the resonance. However, both of these ways are accompanied by the increase of dissipation losses in the media. For practical purposes one has to ensure that the losses do not exceed the nonlinear contribution. To remain in the transparency region $\mathsf{Re}[\chi_{\mathsf{M}}(\omega)] \gg \mathsf{Im}[\chi_{\mathsf{M}}(\omega)]$ the condition $|1 - \omega_r^2/\omega^2| \gg \mathcal{R}_0/\omega L$ must be fulfilled (the overall ohmic resistance R of the whole element is build mostly by the diode resistance $\mathcal{R}_0$). Then the figure of merit for this metastructure takes a simple form

$$\frac{\chi_{\mathsf{M}}^{(2)}(\omega_2; \omega_0, \omega_1) H(\omega_1)}{\mathsf{Im}[\chi_{\mathsf{M}}(\omega_2)]} \sim \frac{|\mathcal{Z}(\omega_2)|}{\mathcal{R}_0} \frac{1 - \omega_r^2/\omega_3^2}{1 - \omega_r^2/\omega_2^2}, \tag{3.18}$$

and its larger values are favourable. This relation shows that choosing one of the frequencies closer to the resonance one can win in the parameters at one frequency, but inevitably loose at the other. The ratio (3.18) appears to be independent of the diode cross-section. Nonlinearity and losses grow equally as the diode gets smaller. Therefore, the only way to improve (3.18) is to increase the ratio $|\mathcal{Z}(\omega)|/\mathcal{R}_0$. As in backward diodes the linear impedance is mostly concerned with the ohmic losses, $|\mathcal{Z}(\omega)| \sim \mathcal{R}_0$, their usage can be limited by significant damping.

A promising opportunity is offered by varactors (see, e.g. Sze, 1981; Helszajn, 1978; Ivanov *et al.*, 1969). For varactors the capacitive impedance can be much higher than the resistance and it is only necessary to ensure that this condition is fulfilled in the desired frequency range.

3.5 Discussion

In summary, we have demonstrated that with the help of simple electronic components it is possible to construct a metamaterial which possesses nonlinear response. We have shown how the macroscopic properties of this material can be controlled by the parameters of the structure elements, their arrangement, and the characteristics of nonlinear insertions. This encourages to expect that various processes, known in nonlinear optics, can be performed in the microwave range with the help of the proposed metamaterial. However, estimates show that in the limit of low nonlinearity a remarkable modulation of the susceptibility is accompanied by substantial dissipation.

Certainly, applying higher pump fields will provide higher nonlinear contribution. However, high nonlinearity would make the susceptibility expansion in the form (3.15) inapplicable, and the corresponding analysis requires an extended approach, which is the subject of the following chapters.

Chapter 4

Three-wave coupling at high nonlinearity

In search for better characteristics we consider below higher amplitudes of the interacting waves, when an essentially nonlinear range of the insertion characteristic is involved. Under this condition a universal description (3.15) of the nonlinear properties of the metamaterial is no longer possible. We have to analyze separately different nonlinear processes and to distinguish between various types of nonlinear insertions.

In this chapter we will concentrate on the three-wave coupling (with frequencies $\omega_\mathrm{p} + \omega_1 = \omega_2$ involved) for a particular class of processes when only one of the waves (at ω_p) is a strong pump wave, while the other two are weak signal waves. Among these are parametric amplification, frequency conversion, parametric instability, etc. We analyze the coupling strength arising with use of nonlinear insertions possessing variable resistance and variable capacitance.

4.1 Coupling strength at high nonlinearity

We have seen in previous chapter (section 3.2, p. 21), that in the metamaterial of RCEs with nonlinear insertions, wave coupling is provided on the level of structure elements. Accordingly, we are first looking for the relationship between currents, induced at the interacting frequencies, analyzing a single element, subjected to oscillating magnetic field.

As in previous, we are concerned with arbitrary flat RCE with effective resistance R, self-inductance L and capacitance C, and take into account the nonlinear insertions, connected in-series to the linear contour.

When the insertions operate in highly nonlinear regime, the resulting time dependencies of voltages and currents in general do not have to be harmonic. In order to deal with harmonic interacting waves in metamaterial, we assume that the contribution of insertions to the response of the structure element is small. Under this assumption, we neglect inharmonicity of the current $I(t)$, driven in RCE by harmonic e.m.f. In following we keep only components, relevant for three-wave coupling, writing the total current as

$$I(t) = \sum_{k=\mathrm{p},\,1}^{2} I^{(k)}(t), \quad I^{(k)}(t) = I_k e^{-i\omega_k t} + \text{c.c.} \tag{4.1}$$

A nonlinear insertion can be generally described with voltage-dependent resistance $\mathcal{R}(U)$ and capacitance $\mathcal{C}(U)$. Then the voltage drop on the insertion $U(t)$, caused by $I(t)$, is

$$U(t) = \mathcal{R}\left(U(t)\right) I(t) + \frac{1}{\mathcal{C}\left(U(t)\right)} \int_{-\infty}^{t} I(\tau)\, d\tau. \tag{4.2}$$

Obviously, even with a harmonic current, this voltage drop is not represented by harmonic oscillations. Therefore, for strong pumping at ω_p we have to assume in general an arbitrary $2\pi/\omega_\mathrm{p}$-periodic time-dependence $U^{(\mathrm{p})}(t)$, having a component at ω_p plus higher harmonics; this dependence can be found for particular insertions as explained below. In contrary, in a linear approximation with respect to weak signal waves, it is sufficient to take into account only the main harmonics of $U(t)$ at ω_1 and ω_2, so that we can summarize the voltage drop, relevant for three-wave coupling, as

$$U(t) = U^{(\mathrm{p})}(t) + \sum_{k=1,2} U^{(k)}(t)$$
$$\text{with} \quad U^{(k)}(t) = U_k e^{-i\omega_k t} + \text{c.c.} \quad \text{only for} \quad k = 1,\, 2. \tag{4.3}$$

Because of nonlinear interaction, the voltages U_k are determined by the currents at all the frequencies involved. In order to determine the coupling strength, we have to express U_k explicitly via these currents. In general, the dependence of $U(t)$ on $I(t)$ is mapped by a functional $U = U\,[I]$, resulting from the solution of a transcendental equation (4.2). Whereas no analytical solution can be obtained for that equation in general, under the assumption of strong pumping $I_\mathrm{p} \gg I_1,\, I_2$ we can perform an expansion with respect to $I_1,\, I_2$, keeping only linear in $I_1,\, I_2$ terms. This results in general coupling equations

$$\begin{aligned} U_2 &= I_2 X_{22}(I_\mathrm{p}) + I_1 X_{21}(I_\mathrm{p}), \\ U_1 &= I_1 X_{11}(I_\mathrm{p}) + I_2 X_{12}(I_\mathrm{p}), \end{aligned} \tag{4.4}$$

where X-factors depend nonlinearly on the pump amplitude; their particular form is determined by characteristics of nonlinear insertions $\mathcal{R}(U)$, $\mathcal{C}(U)$, as discussed in detail in following sections. Provided that we know X-factors, nonlinear coupling between U_1, U_2 and I_1, I_2 is then found.

Next, we return to the response of the whole metamaterial. As before, we consider an array of identical RCEs, arranged as a regular 3D-lattice, so that all the elements lie in parallel planes normal to z axis and all have the same surroundings, and we omit all appearing z and zz indices.

Using the total effective impedance, analogous to (3.9),

$$Z'_{\Sigma}(\omega) = Z(\omega) + \sum_{n' \neq n} Z_{nn'}(\omega) \tag{4.5}$$

(note a remarkable distinction that here only the mutual impedance and the impedance of the linear part of the contour are summed up), for the frequencies of weak signal waves we can write extended impedance equations:

$$\mathcal{E}_k = Z'_{\Sigma}(\omega_k) I_k + U_k, \quad k = 1,\, 2, \tag{4.6}$$

where nonlinear contribution results in additional voltages U_k, given by (4.4) and $\mathcal{E}_k$ implies the e.m.f. (3.7), induced solely by the external field at frequency ω_k.

Now, using (3.7), we combine the systems (4.4) and (4.6), and rewrite them to obtain coupling equations for magnetization of metamaterial, $M(\omega_k)$:

$$M(\omega_2) = \frac{i\omega_2 \aleph S^2 \mathcal{H}(\omega_2) - X_{21} M(\omega_1)}{Z_{\Sigma}(\omega_2) + X_{22}}. \tag{4.7}$$

Here and below we write only ω_2-components for simplicity; expressions for ω_1 are the same except for interchanged indices $1 \leftrightarrow 2$. Using the relation (3.13) that $\mathcal{H} = H + \frac{1}{3}M$, we finally solve (4.7) for M, expressing the magnetization via the macroscopic fields $H(\omega)$ inside metamaterial in the following form:

$$M(\omega_2) = \chi_{\mathsf{M}}(\omega_2) H(\omega_2) + Y(\omega_2; H_{\mathrm{p}}, \omega_{\mathrm{p}}, \omega_1) H(\omega_1). \tag{4.8}$$

The linear magnetic susceptibility here is given by

$$\chi_{\mathsf{M}}(\omega_2) = \frac{\mu_0 \aleph S^2 \omega_2}{-\frac{1}{3}\mu_0 \aleph S^2 \omega_2 - i\left[Z'_{\Sigma}(\omega_2) + X_{22}(I_{\mathrm{p}})\right]}. \tag{4.9}$$

Note that it is modulated due to insertion contribution. Thus, the linear properties of metamaterial at signal frequencies are dependent on the pump field amplitude. This feature represents a valuable tuning effect, which is discussed in detail in the next chapter.

The dimensionless factor

$$Y(\omega_2, H_\mathrm{p}, \omega_\mathrm{p}, \omega_1) = \frac{iX_{21}(I_\mathrm{p})}{\mu_0 \aleph S^2 \omega_2} \cdot \chi_\mathsf{M}(\omega_2)\chi_\mathsf{M}(\omega_1) \tag{4.10}$$

defines the nonlinear modulation of the magnetic susceptibility, and for completeness we have only to express pump current amplitude I_p via pump field amplitude H_p. For the strong pumping at one frequency, an additional nonlinear contribution from signal waves to $M(\omega_\mathrm{p})$ and to $\chi_\mathsf{M}(\omega_\mathrm{p})$ can be neglected, so that $M(\omega_\mathrm{p}) = \chi_\mathsf{M}(\omega_\mathrm{p})H(\omega_\mathrm{p})$ and then

$$I_\mathrm{p} = \frac{\chi_\mathsf{M}(\omega_\mathrm{p})}{\aleph S} H_\mathrm{p}. \tag{4.11}$$

Equation (4.10) with relation (4.11) describe then the strength of nonlinear coupling between the interacting waves.

The expression (4.8) is analogous to (3.15), with a notable distinction that the dependence of nonlinear modulation on H_p is no longer linear, but is included in the modulation coefficient $Y(\omega_2; H_\mathrm{p}, \omega_\mathrm{p}, \omega_1)$ via X_{21}-factor. In the limit of weak nonlinearity, X-factors can be easily calculated analytically, leading to the linear dependence on H_p in agreement with Eq. (3.15), obtained in Chapter 3, and then Eq. (4.9) coincide with Eq. (3.14), and Eq. (4.10) yields Eq. (3.16), multiplied by $H(\omega_\mathrm{p})$.

Considering application capabilities of metamaterial, it is important to keep in mind that energy dissipation can be essential, especially for the insertions with variable resistance. For nonlinear coupling in the form (4.8), the rate of the energy exchange between the interacting waves depends on the modulation coefficient Y, whereas the wave energy dissipation is determined by the imaginary part of the linear susceptibility. Therefore, in order to enable efficient nonlinear processes, $\mathsf{Im}[\chi_\mathsf{M}(\omega)]$ should not exceed Y. Provided that the contribution of insertions is small compared to the linear contour response, we can safely assume that the overall dissipation is small and $\mathsf{Im}[\chi_\mathsf{M}(\omega)] \ll \mathsf{Re}[\chi_\mathsf{M}(\omega)]$. This entitles us to use an approximation

$$\mathsf{Im}[\chi_\mathsf{M}(\omega_2)] \approx |\chi_\mathsf{M}(\omega_2)|^2 \cdot \frac{\mathsf{Re}[X_{22}]}{\mu_0 \aleph S^2 \omega_2}, \tag{4.12}$$

where we also imply that the resistance R of the linear part of the RCE contour is negligible compared to that of the insertion, $\mathsf{Re}[X_{22}]$.

In following sections we analyze the details of calculating X-factors for particular types of insertions and estimate the magnitudes of nonlinear modulation, achievable with use of nonlinear devices, reported in literature.

4.2 Insertions with variable resistance

4.2.1 Nonlinear modulation

Analyzing the behaviour of a diode with variable resistance, inserted into a RCE, we can simplify the general equation (4.2), which lacks capacitive term for this case, immediately describing the current-voltage characteristic by an arbitrary function $\mathcal{U}(I)$. This function can be approximated analytically or mapped using direct measurements for a particular insertion. The voltage drop on the insertion is then determined by this function, taken with I given by (4.1). Expanding it up to linear with respect to I_1, I_2 terms, we obtain

$$U(t) = \mathcal{U}\left(I^{(\mathrm{p})}(t)\right) + \mathcal{U}'\left(I^{(\mathrm{p})}(t)\right) \cdot (I_1 e^{-i\omega_1 t} + I_2 e^{-i\omega_2 t} + \text{c.c.}), \tag{4.13}$$

where $\mathcal{U}'$ denotes $d\mathcal{U}/dI$. Combining together all the terms with ω_2, we arrive directly at the form (4.4), e.g.,

$$U_2 = I_2 X_{22}(I_\mathrm{p}) + I_1 X_{21}(I_\mathrm{p}) \tag{4.14}$$

where the X-factors can be calculated, for a given $\mathcal{U}(I)$ dependence, as zero and first Fourier coefficients of $\mathcal{U}'\left(I^{(\mathrm{p})}(t)\right)$ function:

$$X_{22}(I_\mathrm{p}) = \frac{\omega_\mathrm{p}}{2\pi} \int\limits_0^{2\pi/\omega_\mathrm{p}} \mathcal{U}'\left(I^{(\mathrm{p})}(t)\right)\, dt, \tag{4.15}$$

$$X_{21}(I_\mathrm{p}) = \frac{\omega_\mathrm{p}}{2\pi} \int\limits_0^{2\pi/\omega_\mathrm{p}} \mathcal{U}'\left(I^{(\mathrm{p})}(t)\right) e^{-i\omega_\mathrm{p} t}\, dt. \tag{4.16}$$

Then the nonlinear modulation (4.10) and dissipation (4.12) can be obtained for particular insertion characteristics and metamaterial parameters.

4.2.2 Practical estimates for backward diodes

To make use of variable resistance, we suggest to employ backward diodes. They are notable for high sensitivity, which would enable relatively low pump amplitudes, and are commonly used in the operational range around zero voltage, requiring no additional bias.

The characteristics of particular backward diodes may vary essentially, but here we would like to give merely qualitative estimates. To choose yet some particular parameters we refer to a typical set of InGaAs diodes, reported by Schulman *et al.* (2001) to be designed for high nonlinearity. The current-voltage characteristics demonstrated there have different appearance, but what is essential for nonlinear effects is the curvature of the current-voltage dependence, while the scaling along either axis *per se* is not relevant for comparative analyzis.

Accordingly, we model a set of current-voltage characteristics by functions $\mathcal{I}(U)$, which show qualitative agreement with the experimental curves (Schulman *et al.*, 2001) within the intended operating range (Fig. 4.1a). All the functions have the same initial slope, corresponding to $10\,\Omega$ zero-bias resistance (which implies 10^{-2}–$10^{-3}\,\mathrm{mm}^2$ diode cross-section).

To calculate the X-factors, we imply, in accordance with the above assumptions that the diode in RCE is forced to external harmonic pump current $I^{(\mathrm{p})}(t)$, and for this current we obtain the $U(t)$ by solving an equation $\mathcal{I}\left(U(t)\right) = I^{(\mathrm{p})}(t)$ numerically.

To estimate the resulting nonlinear modulation (4.10), we take an example of metamaterial with circular RCEs with 5 mm radius and 1 mm wire diameter, arranged in parallel planes with tetragonal symmetry with 2.2 radii in-layer spacing and half-radius inter-layer spacing. Such RCE dimensions provide self-inductance of about 12 nH; choosing contour capacitance about 0.02 pF we arrive at single element resonance frequency of $2\pi \cdot 10^{10}\,\mathrm{rad/s}$. With the above lattice constants, resonance frequency of the effective magnetic susceptibility occurs at $1.2\pi \cdot 10^{10}\,\mathrm{rad/s}$. We assume that the metamaterial is employed below the resonance, so that $\chi_{\mathsf{M}}(\omega_1)$, $\chi_{\mathsf{M}}(\omega_2)$ are of the order of unity. This corresponds to the wavelengths of the order of 10 cm, quite acceptable for the chosen RCE size.

In Fig. 4.1b we plot the nonlinear modulation $|Y(\omega_2, H_\mathrm{p}, \omega_\mathrm{p}, \omega_1)|$ as a function of pump field amplitude H_p, for each of modelled current-voltage characteristics shown in Fig. 4.1a. It is remarkable that these dependances have qualitatively different appearance: for the characteristics having a “negative resistance” range (Fig. 4.1a, solid and dash lines) a sharp pronounced maxima are obtained, while for those being monotonous ones (Fig. 4.1a, dot and dash-dot lines) the maxima are smooth.

Such behaviour is expected from the expression (4.16) for X_{21} factor, responsible for nonlinearity. Indeed, this factor is determined by the integration over $\mathcal{U}'(I)$ values. The current-voltage characteristics of the first type have points I_∞ where $\mathcal{U}'(I)$ tends to infinity. They correspond to unstable states of the diode, so when the current amplitude is larger than I_∞, they are rapidly crossed by $I(t)$ in a hysteresis-like way, and do not contribute much to the integral. However, the closer is the amplitude to I_∞, the more time the diode spends in the state with high $\mathcal{U}'(I)$ values (because the oscillating $I(t)$ is around the turning point there). In an ideal case, when I_p matches I_∞

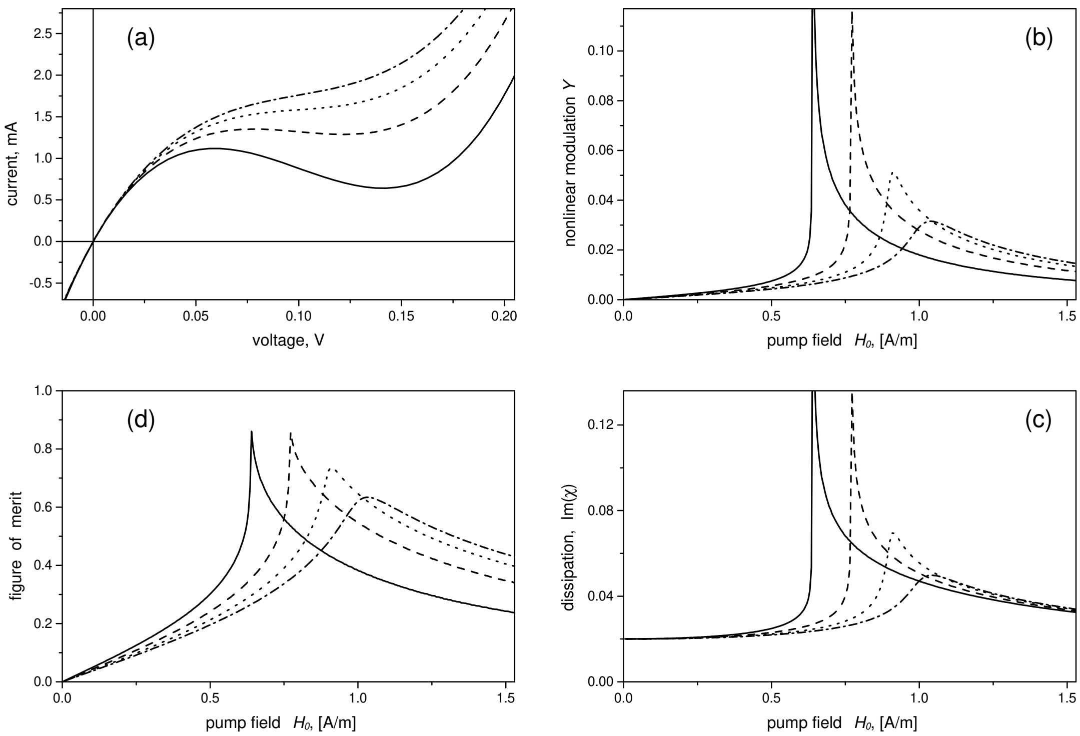

Figure 4.1: Backward diodes as nonlinear insertions: (a) model current-voltage characteristics; corresponding dependances on the pump field amplitude H_p of (b) nonlinear modulation Y, (c) dissipation $\mathsf{Im}[\chi_\mathsf{M}(\omega)]$, and (d) figure of merit $Y/\mathsf{Im}[\chi_\mathsf{M}(\omega)]$.

exactly, X_{21} would tend to infinity, and so would the nonlinear modulation. Obviously, this condition cannot be reached in reality due to unavoidable inhomogeneity of the diodes, RCEs, their arrangement, etc., otherwise negligible. Moreover, significant increase in effective diode resistance for signal waves would make the above approach inappropriate, as the requirement of weak insertion contribution would not hold. In principle, this situation could give rise to numerous interesting effects, investigation of which is, however, beyond the aim of this thesis. Supposing that all the limitations would not allow extremely high X-factors, we still expect that nonlinearity observed in real systems will be rather sensitive to the pump amplitude in the narrow range around I_∞.

In contrary, for monotonous characteristics no such peculiarities are expected, and smooth maxima are reached when the current amplitudes are in the range where $\mathcal{U}'(I)$ has maximal values.

As seen from Fig. 4.1b, an exceptionally high nonlinear modulation, about 0.05 and more, can be achieved with moderate pump fields, about 1 A/m.

Note that the X_{22}-factor (4.15), responsible for dissipation in the metamaterial, also involves the integration over $\mathcal{U}'(I)$. Therefore, $\mathsf{Im}[\chi_\mathsf{M}(\omega)]$ (4.12) show similar behaviour with respect to pump amplitudes (Fig. 4.1c). In the limit of zero pumping, it is determined by zero-bias resistance, as expected.

The results in Fig. 4.1b and Fig. 4.1c show that both nonlinearity modulation Y and dissipation, characterized by $\mathsf{Im}[\chi_\mathsf{M}(\omega)]$, have not only qualitatively similar dependence on I_p, but also reach comparable magnitudes. In Fig. 4.1d we plot the ratio $|Y(\omega_2, H_\mathrm{p}, \omega_\mathrm{p}, \omega_1) \,/\, |\mathsf{Im}[\chi_\mathsf{M}(\omega_2)]$, which represents a kind of figure of merit. This ratio appear to be below unity for all the current-voltage characteristics; this is not surprising in view of the resistive nature of the nonlinearity. This feature might limit the application of backward diodes in metamaterials designed for nonlinear processes concerned with wave coupling. On the other hand, it is quite useful for other applications like band gap tuning (see Chapter 5).

Insertions with variable capacitance, which are discussed below, possess a different nonlinearity origin and are, therefore, free from this limitation.

4.3 Insertions with variable capacitance

4.3.1 Nonlinear modulation

We assume such an insertion to possess a voltage-dependent capacitance $\mathcal{C}(U)$ and constant resistive losses $\mathcal{R}$. Despite the latter holds only for particular varactors (e.g. Mamor *et al.*, 2001), as far as the quality factor is high at the frequencies concerned, $\mathcal{R} \ll |1/(\omega\mathcal{C})|$ and the resistance would not provide remarkable contribution to nonlinear modulation. Thus, we neglect $\mathcal{R}(U)$ dependence in (4.2) for simplicity. Then the voltage drop at the insertion obeys the equation

$$U(t) = \mathcal{R}I(t) + \frac{1}{\mathcal{C}\left(U(t)\right)} \int\limits_{-\infty}^{t} I(\tau)\, d\tau. \tag{4.17}$$

and we have to analyze it with current (4.1) and voltage (4.3). We remind that the pumping is expected to be only slightly distorted by the insertion, so that $I^{(\mathrm{p})}(t) \gg I^{(1,2)}(t)$ and $U^{(\mathrm{p})}(t) \gg U^{(1,2)}(t)$. Therefore, in order to determine the voltage drop, caused by pumping, we take into account only $U^{(\mathrm{p})}(t)$ and harmonic $I^{(\mathrm{p})}(t)$ in Eq. (4.17). Then we arrive at a transcendental equation

$$U^{(\mathrm{p})}(t) = \mathcal{R} \cdot \left(I_{\mathrm{p}} e^{-i\omega_{\mathrm{p}} t} + \text{c.c.}\right) + \frac{1}{\mathcal{C}\left(U^{(\mathrm{p})}(t)\right)} \left(\frac{I_{\mathrm{p}} e^{-i\omega_{\mathrm{p}} t}}{-i\omega_{\mathrm{p}}} + \text{c.c.}\right), \tag{4.18}$$

which can be solved numerically for a given $\mathcal{C}(U)$ dependence. In general, this results in $U^{(\mathrm{p})}(t)$ having components at ω_{p} and its multiples.

Next, considering (4.17) for signal components, in the linear approximation we can perform an expansion

$$\frac{1}{\mathcal{C}\left(U(t)\right)} \approx \frac{1}{\mathcal{C}\left(U^{(\mathrm{p})}(t)\right)} + \left(\frac{1}{\mathcal{C}\left(U^{(\mathrm{p})}(t)\right)}\right)' \cdot \left(U_1 e^{-i\omega_1 t} + U_2 e^{-i\omega_2 t} + \text{c.c.}\right), \tag{4.19}$$

where we denote

$$\left(\frac{1}{\mathcal{C}\left(U^{(\mathrm{p})}(t)\right)}\right)' \equiv \frac{d}{dU} \left(\frac{1}{\mathcal{C}(U)}\right)\Bigg|_{U=U^{(\mathrm{p})}(t)}.$$

For a known $U^{(\mathrm{p})}(t)$ function, both fractions in (4.19) can be written as corresponding Fourier expansions:

$$\begin{aligned} \frac{1}{\mathcal{C}\left(U^{(\mathrm{p})}(t)\right)} &= \sum_{n=0}^{\infty} K_n e^{-in\omega_{\mathrm{p}} t} + \text{c.c.}, \\ \left(\frac{1}{\mathcal{C}\left(U^{(\mathrm{p})}(t)\right)}\right)' &= \sum_{n=0}^{\infty} G_n e^{-in\omega_{\mathrm{p}} t} + \text{c.c.}, \end{aligned} \tag{4.20}$$

with Fourier coefficients

$$
\begin{aligned}
K_n &= \frac{\omega_\mathrm{p}}{2\pi} \int\limits_0^{2\pi/\omega_\mathrm{p}} \frac{1}{\mathcal{C}\left(U^{(\mathrm{p})}(t)\right)} e^{-in\omega_\mathrm{p} t}\, dt \\
G_n &= \frac{\omega_\mathrm{p}}{2\pi} \int\limits_0^{2\pi/\omega_\mathrm{p}} \left(\frac{1}{\mathcal{C}\left(U^{(\mathrm{p})}(t)\right)}\right)' e^{-in\omega_\mathrm{p} t}\, dt.
\end{aligned}
\tag{4.21}
$$

Now we can insert the obtained expansions (4.20) into Eq. (4.17), and combine the terms contributing at ω_1 and ω_2, taking $\omega_\mathrm{p} + \omega_1 = \omega_2$ into account. Keeping only linear with respect to I_1, I_2, U_1, U_2 terms provides us with the linear system of equations

$$
\begin{cases}
U_1 = \mathcal{R} I_1 + G_0 \left(\dfrac{I_\mathrm{p}^*}{i\omega_\mathrm{p}}\right) U_2 + G_1^* \left(-\dfrac{I_\mathrm{p}}{i\omega_\mathrm{p}}\right) U_1 + G_1 \left(\dfrac{I_\mathrm{p}^*}{i\omega_\mathrm{p}}\right) U_1 \\
\qquad\qquad + K_0 \left(-\dfrac{1}{i\omega_1}\right) I_1 + K_1^* \left(-\dfrac{1}{i\omega_2}\right) I_2, \\
U_2 = \mathcal{R} I_2 + G_0 \left(-\dfrac{I_\mathrm{p}}{i\omega_\mathrm{p}}\right) U_1 + G_1^* \left(-\dfrac{I_\mathrm{p}}{i\omega_\mathrm{p}}\right) U_2 + G_1 \left(\dfrac{I_\mathrm{p}^*}{i\omega_\mathrm{p}}\right) U_2 \\
\qquad\qquad + K_0 \left(-\dfrac{1}{i\omega_1}\right) I_2 + K_1 \left(-\dfrac{1}{i\omega_2}\right) I_1.
\end{cases}
\tag{4.22}
$$

The algebraic system (4.22) can be solved straightforwardly, enabling to express U_2 via I_1 and I_2 in the form (4.4), with the X-factors given, upon algebraic simplification, by

$$
X_{21} = \frac{\omega_\mathrm{p}}{\omega_1} \frac{G_0 I_\mathrm{p} (K_0 - i\omega_1 \mathcal{R}) - K_1 (i\omega_\mathrm{p} - G_1 I_\mathrm{p}^* + G_1^* I_\mathrm{p})}{(i\omega_\mathrm{p} - G_1 I_\mathrm{p}^* + G_1^* I_\mathrm{p})^2 + G_0^2 I_\mathrm{p} I_\mathrm{p}^*}, \tag{4.23}
$$

$$
X_{22} = \frac{\omega_\mathrm{p}}{\omega_2} \frac{G_0 I_\mathrm{p} K_1 - (K_0 - i\omega_2 \mathcal{R})(i\omega_\mathrm{p} - G_1 I_\mathrm{p}^* + G_1^* I_\mathrm{p})}{(i\omega_\mathrm{p} - G_1 I_\mathrm{p}^* + G_1^* I_\mathrm{p})^2 + G_0^2 I_\mathrm{p} I_\mathrm{p}^*}. \tag{4.24}
$$

Then the nonlinear modulation (4.10) and dissipation (4.12) can be calculated for particular metamaterial parameters.

4.3.2 Practical estimates for varactors

Non-symmetric varactor diodes

Obviously, varactors, appropriate for practical realization of the three-wave coupling, have to possess a non-symmetric capacitance-voltage characteristic. An overview of recent publications (Fu *et al.*, 2000; Lebedev and Polyakov, 2000; Mamor *et al.*, 2001; Marso *et al.*, 2001; Abadei *et al.*, 2002) and review papers (Kollberg *et al.*, 1996; Vanbésien *et al.*, 1999) allows us to infer that such devices are available for application in GHz range with the quality factors good enough. Without going into details of particular data, in the illustrative estimates below we rely on typical parameters (Mamor *et al.*, 2001) and model capacitance-voltage characteristics by a set of algebraic $\mathcal{C}(U)$ functions (Fig. 4.2a). We assign the same zero-bias capacitance $\mathcal{C}_0 = 0.2\,\mathrm{pF}$ (so that $\mathcal{C}_0 \gg C$) and the same sensitivity to voltage to all the functions, as changing these parameters results only in scaling without qualitative difference in the nonlinear response we are looking for. Instead, we vary the ratio of the capacitance $\mathcal{C}_1$, corresponding to a certain large voltage, to $\mathcal{C}_0$.

In Fig. 4.2b we plot the nonlinear modulation as a function of pump field amplitude, calculated for each of the modelled functions. It shows significant increase as the pump amplitude exceeds certain value. It is notable that the sensitivity of nonlinear modulation to the pumping depends remarkably on the $\mathcal{C}_1/\mathcal{C}_0$ ratio, with $Y(H_\mathrm{p})$ being much steeper for a merely 2–3 times lower ratio. With the accepted practical parameters (see Section 4.2.2) we estimate that enormous nonlinear modulation of the order of 0.1 is achievable with quite feasible field amplitudes, about 0.2 – 0.5 A/m.

The data in Fig. 4.2 suggest even higher modulation, but this is not acceptable within the frame of approach presented here. Already a 10% modulation is incomparably higher than the magnitudes known in optics. This implies that such a metamaterial can be effective with by far less optimal parameters than those taken for estimates here.

For comparison, we also plot $\mathsf{Im}[\chi_\mathsf{M}(\omega)]$, assuming the quality factor of varactor itself to be about 100 (Fig. 4.2b, grey line). We see that dissipation does not depend markedly on the pumping, which is not surprising when $\mathcal{R}(I)$ dependence is negligible. This means, in particular, that with poorer quality factors nonlinear modulation that exceeds losses still can be obtained, though with more intense pumping.

Despite these promising estimates, varactor diodes have some disadvantages. Namely, they experience avalanche breakdown at moderate voltage, and they often have subdued performance at high frequencies. This limits either suitable field amplitudes and therefore, achievable nonlinearity, or the range of operating frequencies.

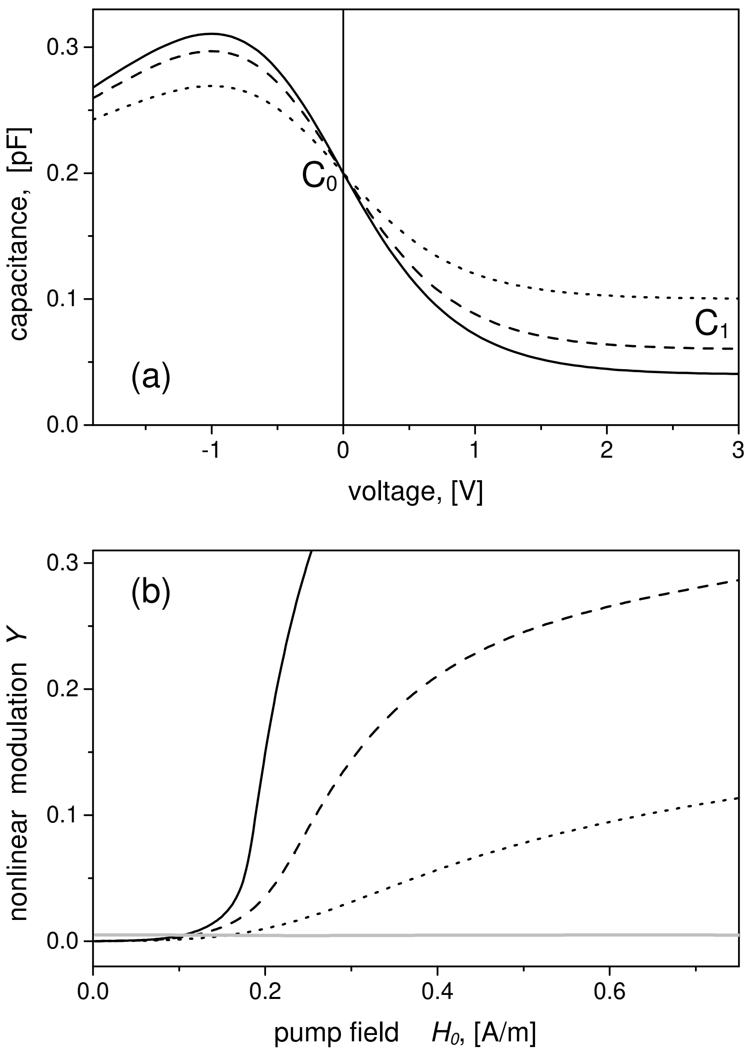

Figure 4.2: Varactor diodes as nonlinear insertions: (a) model capacitance-voltage characteristics with $\mathcal{C}_1/\mathcal{C}_0$ ratios 0.2 (solid), 0.3 (dash), 0.5 (dot); (b) corresponding nonlinear modulation $Y(H_\mathrm{p})$ and dissipation $\mathsf{Im}[\chi_\mathsf{M}(\omega)]$ (grey line).

Varactors based on ferroelectric films

The aforementioned disadvantages of varactors are overcome in variable capacitance devices based on ferroelectric films (Kozyrev *et al.*, 2000; Cho *et al.*, 2002; Canedy *et al.*, 2001; York *et al.*, 2001; Li *et al.*, 2001; Tappe *et al.*, 2003; Razumov *et al.*, 2003). These can tolerate much higher voltages and can be employed at frequencies up to THz range, which are even higher than presently intended for metamaterials. However, varactors based on ferroelectric films possess symmetric capacitance-voltage characteristics, and therefore require an additional bias in order to be employed in three-wave coupling processes.

A conventional for electronics way to bias a diode by means of external voltage supply might be acceptable for a single RCE or a planar configuration used by Reynet and Acher (2004), but is hardly ever realizable in 3-D metamaterials. We propose, instead, to bias the diode with a voltage drop caused by e.m.f., induced in RCE by additional external magnetic field $H_{\mathrm{b}}(t)$, varying at times much larger than the period of the interacting signals.

From typical data (York *et al.*, 2001), we rely on in the estimates below, we presume that the required bias voltage U_{b} is of the order of volts. To estimate the corresponding external biasing field we note that for slowly varying field, the induced e.m.f. $\mathcal{E}_{\mathrm{b}}(t) = -\mu_0 S\dot{H}_{\mathrm{b}}(t)$ entirely results in voltage drops on the capacitances C of the RCE contour and $\mathcal{C}(U_{\mathrm{b}})$ of the diode. Then the voltage on the diode is given by

$$U_{\mathrm{b}} = -\frac{C}{\mathcal{C}(U_{\mathrm{b}}) + C}\,\mu_0 S\dot{H}_{\mathrm{b}},$$

where characteristic $\dot{H}_{\mathrm{b}}$ amplitudes are obtained from. With $\mathcal{C}(U_{\mathrm{b}})/C \sim 10$ we arrive at $\dot{H}_{\mathrm{b}} \sim 10^{-11}\,\mathrm{A/(m\cdot s)}$, which means, for instance, fields about $1000\,\mathrm{A/m}$ varying at characteristic time about $10\,\mathrm{ns}$.

For a qualitative illustration, we model $\mathcal{C}(U)$ dependances, similar to those reported by York *et al.* (2001), with simple functions, shifted (biased) from symmetrical with respect to $U = 0$ position. The maximal capacitance $\mathcal{C}_0$ is kept same for all the functions, while either "minimal" capacitance $\mathcal{C}_1$ (Fig. 4.3a) or bias (Fig. 4.4a), are variable parameters. The corresponding dependances of the nonlinear modulation on the pump field intensity, calculated for these sets of functions, are plotted in Fig. 4.3b and Fig. 4.4b, respectively. We do not plot $\mathsf{Im}[\chi_{\mathsf{M}}(\omega)]$ there, as it demonstrates similar behaviour as in Fig. 4.2, being much smaller than the achievable nonlinearity.

Fig. 4.3b shows that the nonlinear modulation grows essentially with increasing pump amplitude above certain value, which is independent of $\mathcal{C}_1/\mathcal{C}_0$ ratio, while the rate of nonlinearity growth is remarkably sensitive to this

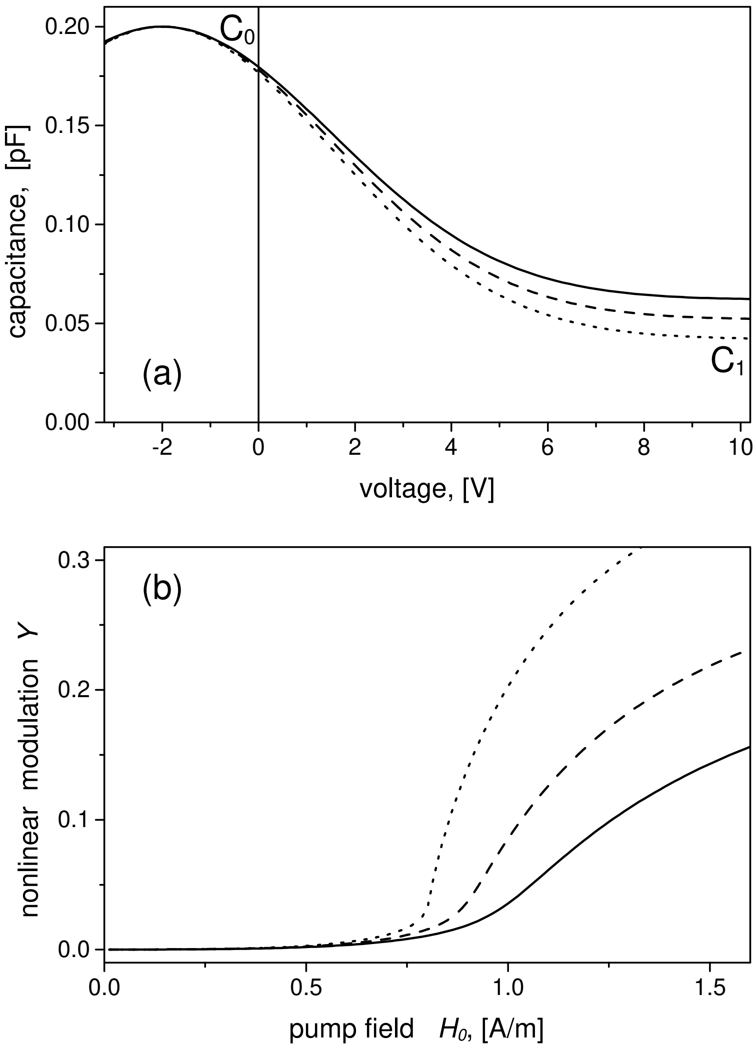

Figure 4.3: Biased ferroelectric films as nonlinear insertions: (a) model capacitance-voltage characteristics, with $\mathcal{C}_1/\mathcal{C}_0$ ratios 0.2 (solid), 0.25 (dash), 0.3 (dot); (b) corresponding nonlinear modulation $Y(H_{\rm p})$.

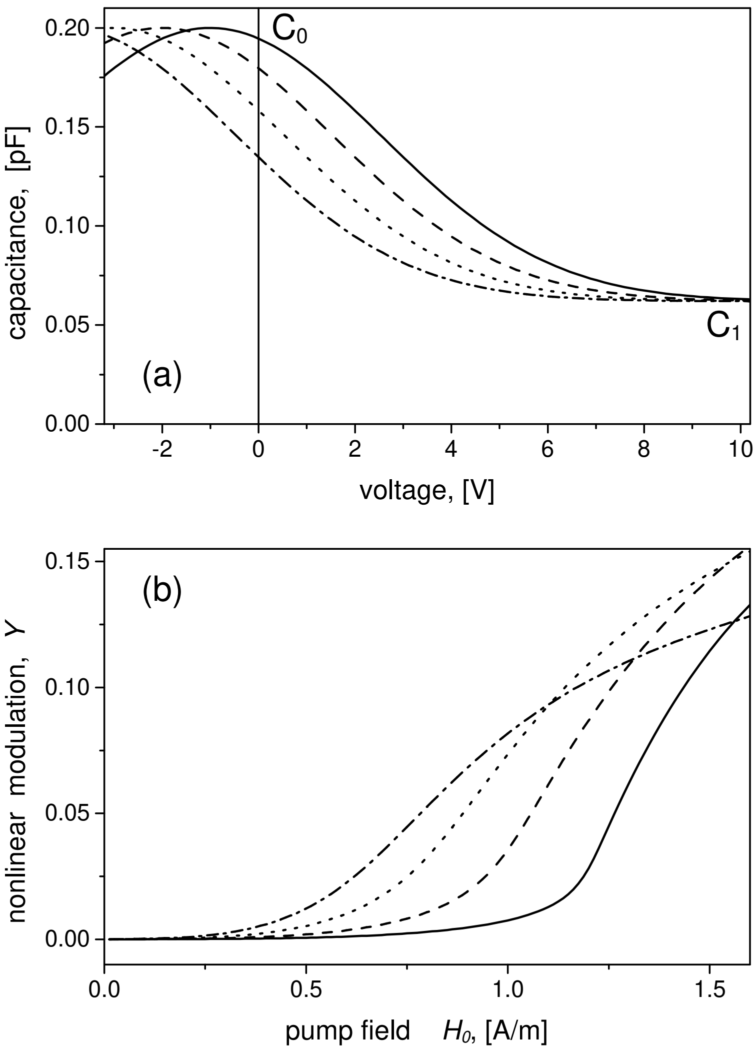

Figure 4.4: Controlling nonlinearity by bias: (a) model capacitance-voltage characteristics ($\mathcal{C}_1/\mathcal{C}_0 = 0.3$); (b) corresponding nonlinear modulation $Y(H_{\rm p})$. Ferroelectric films are biased by 1 V (solid), 2 V (dash), 3 V (dot), 4 V (dash-dot).

ratio. This pattern is analogous to what occurs for non-symmetric varactor diodes; it is not surprising, as the model $\mathcal{C}(U)$ functions are qualitatively similar in these two cases. The exceptional modulation of the order of 0.1 is reached here at larger pump amplitudes, in accordance with higher operating voltages for devices based on ferroelectric films.

Increasing bias, as shown in Fig. 4.4b, results in lower pump fields required to achieve essential nonlinearity. This enables controlling the strength of nonlinear coupling: varying biasing field with a fixed pump intensity leads to significant change in nonlinear modulation. Such tuning of the nonlinear response has no direct analogy in optical crystals and represents an example of advantageous metamaterial's controllability.

4.4 Discussion

We developed an approach for calculating nonlinear modulation of magnetic susceptibility in the metamaterial with the insertions operating in essentially nonlinear regime. We have shown that the dependence of the modulation on the pump field amplitude is remarkably nonlinear, with the peculiarities determined by the type of insertion and its particular characteristics.

Practical estimates, relying on the diodes' characteristics, taken from contemporary publications, predict that while using rather moderate pump fields (about 1 A/m or less), incredibly high nonlinear modulation of magnetic susceptibility, up to 0.1, can be achieved. Such an enormous value exceeds by many orders of magnitude nonlinearities, known in optics. Note that in illustrative examples we neither claim to have chosen optimal insertion properties, nor intend to suggest necessarily the particular diodes, mentioned above, for practice. We rather propose a universal method for deriving metamaterial properties from the known characteristics of insertions, whichever appear appropriate for experiment. General recommendations for choosing them, however, can be acquired already from the illustrations here.

We point out a valuable advantage that in the considered metamaterial nonlinear response can be tuned by external varying magnetic field. This feature, having no direct analogy in optics, can offer additional improvements to conventional nonlinear applications as well as new unusual techniques.

We believe that the approach, developed here, represents the basics for analyzis of metamaterials with nonlinear insertions, and that it can be further extended in order to describe other kinds of nonlinear processes.

Chapter 5

Band gap tuning

5.1 Tunability of nonlinear metamaterial

5.1.1 Introduction

In this chapter we study tuning of the metamaterial permeability by an external varying magnetic field. This field induces voltages in RCEs, which bias the nonlinear insertions and vary the effective capacitance and/or resistance of RCEs. This results in changes of the RCEs' resonant frequency and quality factor, which in turn affect the resonant frequency and resonance width of the metamaterial permeability. The latter determines the band gap and controls the propagation of weak signal waves through the medium. Then, the metamaterial can be switched between transmitting, reflecting, and absorbing states.

Particular tuning capabilities depend strongly on the type of the nonlinear insertion. For instance, insertions with variable resistance allow affecting the effective RCE resistance and provide a tuning of the material transparency, i.e., switching between transmitting and absorbing states. Variable capacitance insertions allow varying the effective RCE capacitance, which defines the position of the metamaterial resonance. Shifting the resonance one can switch the medium between all the three states with respect to a signal wave at a given frequency.

We propose two tuning regimes: tuning by a strong slow varying field and tuning by a high-frequency field. With the slow tuning, the refractive index of the metamaterial is changed adiabatically, following time derivatives of the external field. With the high-frequency tuning, a strong pump microwave propagating through the medium causes a homogeneous variation of the refractive index, which can be controlled by adjusting the wave amplitude and/or frequency.

To estimate arising application possibilities we study microwave transmission through a slab of the nonlinear metamaterial. We show that even a relatively thin slab, having the thickness equal to one microwave wavelength in vacuum, can be used for a modulation of the transmitted signal microwave amplitude by several orders of magnitude.

5.1.2 Controlling RCE properties

We describe the parameters of the linear part of RCE with resistance R_c, self-inductance L_c and capacitance C_c, where index c is added for the ease of notation throughout this chapter. Nonlinear insertion is generally characterized with resistance and capacitance, depending on the voltage drop on the insertion, $\mathcal{R}(U)$ and $\mathcal{C}(U)$, respectively, keeping the notation of Chapter 4.

With an insertion, operating in essentially nonlinear regime (see section 4.1), the current $I(t)$ in the RCE, induced by an external electromotive force $\mathcal{E}(t)$, obeys the equation

$$\mathcal{E}(t) = R_c I(t) + \frac{1}{C_c}\int\limits_{-\infty}^{t} I(\tau)\, d\tau + L_c \dot{I}(t) + U(t), \tag{5.1}$$

where the voltage drop on the insertion is given by (4.2):

$$U(t) = I(t)\mathcal{R}\left(U(t)\right) + \frac{1}{\mathcal{C}\left(U(t)\right)}\int\limits_{-\infty}^{t} I(\tau)\, d\tau. \tag{5.2}$$

While considering the tuning phenomena, we focus on the effect of strong pump field on the propagation of weak harmonic signal wave, which probes the changes of linear metamaterial response at frequency ω. Correspondingly, we separate the current and voltage into pump (index p) and signal (index ω) components:

$$I(t) = I_{\mathrm{p}}(t) + I_\omega e^{-i\omega t} + I_\omega^* e^{i\omega t}, \quad U(t) = U_{\mathrm{p}}(t) + U_\omega e^{-i\omega t} + U_\omega^* e^{i\omega t}. \tag{5.3}$$

For the signal terms much smaller than the pumping ones, it is possible to perform an expansion in (5.2). In the zero order approximation, with the signal contribution being neglected, Eq. (5.2) allows to determine the pump voltage for a given pump current. Next, in the linear approximation with respect to the signal, the signal voltage is proportional to the signal current, $U_\omega \propto I_\omega$. It is convenient to separate the real and imaginary parts of the proportionality factor and write:

$$U_\omega = \left(\mathcal{R}(t) + \frac{i}{\omega\mathcal{C}(t)}\right) I_\omega. \tag{5.4}$$

Here the effective insertion capacitance and resistance vary in time due to the pumping. The particular form of Eq. (5.4) is determined by the type of nonlinear insertion and the regime of tuning, as discussed in detail in Sections 5.2 and 5.3.

Considering the harmonic signal, we obtain from Eq. (5.1)

$$\mathcal{E}_\omega = Z_c(\omega)I_\omega + U_\omega, \tag{5.5}$$

where $Z_c(\omega) = R_c - i\omega L_c + i(\omega C_c)^{-1}$ is the linear RCE impedance and $\mathcal{E}_\omega$ is the electromotive force at the signal wave frequency. Substituting the relation (5.4) in (5.5) yields that an RCE with nonlinear insertion acquires an effective impedance

$$Z(t) = R(t) - i\omega L_c + i\left(\omega C(t)\right)^{-1}, \tag{5.6}$$

which is affected by the pumping through the overall resistance $R(t) = R_c + \mathcal{R}(t)$ and capacitance $C(t) = \left(C_c^{-1} + \mathcal{C}^{-1}(t)\right)^{-1}$. Therefore, the main RCE characteristics, its resonant frequency, $\omega_0 = (L_c C)^{-1/2}$, and quality factor, $Q = R^{-1}\sqrt{L_c/C}$, are tuned by pumping.

5.1.3 Macroscopic parameters and band gap

Metamaterial made of RCEs has rather trivial electric properties: its permittivity is positive and shows no notable frequency dispersion. Magnetic properties of such structure, as shown in Chapter 2, are described with diagonal tensor of effective permeability with components:

$$\mu_{xx} = 1, \quad \mu_{yy} = 1, \quad \mu_{zz}(\omega) = 1 - \frac{A\omega^2}{\omega^2 - \omega_r^2 + i\Gamma\omega}. \tag{5.7}$$

We remind that the resonant frequency (2.25),

$$\omega_r = \omega_0 \left(\frac{L_\Sigma}{L} + \frac{1}{3}\frac{\mu_0 \aleph S^2}{L} \right)^{-1/2}, \tag{5.8}$$

is shifted from ω_0 due to mutual interaction of structure elements. The resonance height and width are given by (2.25) and (2.26), respectively.

As follows from Eq. (5.7), propagation conditions for electromagnetic waves with magnetic field directed along z-axis, substantially depend on the wave frequency. Namely, the medium is:

- transparent at ω lower than ω_r, where $\mathsf{Re}[\mu_{zz}] > 0$ and $\mathsf{Im}[\mu_{zz}] \ll 1$;

- absorptive at frequencies close to the resonance, $|\omega - \omega_r| \leq \Gamma$, where $\mathsf{Re}[\mu_{zz}] \sim \mathsf{Im}[\mu_{zz}]$ and incident waves dissipate in the bulk;
- reflecting in a certain band gap above ω_r, where $\mathsf{Re}[\mu_{zz}] < 0$ and $\mathsf{Im}[\mu_{zz}] \ll 1$, and incident waves are reflected from the surface.
- transparent above the band gap, where $\mathsf{Re}[\mu_{zz}] > 0$ and $\mathsf{Im}[\mu_{zz}] \ll 1$.

In order to achieve maximal tuning effect, it is desirable to adjust the metamaterial resonance close to the frequency of the incident signal wave. Then by varying the parameters ω_r (by shifting ω_0) and/or Γ (by changing Q) it is possible to affect drastically band gap parameters. Note that large values of the real part of the permeability at such frequencies lead to high refractive index. This reduces wavelengths and electromagnetic penetration depths inside the metamaterial. Therefore, already thin slab can be used for significant modulation of the signal.

5.2 Tuning by slowly varying field

Adiabatic tuning of the metamaterial can be accomplished by applying a slowly varying external magnetic field. All the three tensor components of the permeability (5.7) are equal or close to unity at small frequencies. Therefore, pump field inside the medium, $H_{\mathrm{p}}(t)$, equals to the externally applied one. We assume the latter to be homogeneous and perpendicular to RCE planes (parallel to z-axis). The electromotive force induced in RCE by the external field,

$$\mathcal{E}_{\mathrm{p}}(t) = -\mu_0 S \dot{H}_{\mathrm{p}}(t), \tag{5.9}$$

drives pump current, which, in turn, gives rise to pump voltages biasing the nonlinear insertion. The resulting tuning effect depends on the type of the insertion. Below we consider particular cases of variable resistance and variable capacitance insertions.

5.2.1 Variable resistance

For variable resistance devices, the capacitive contribution in Eq. (5.2) is not relevant, and their properties are usually described by current-voltage characteristic. Here we consider the reciprocal, voltage-current, characteristic $\mathcal{U}(I)$. Then, instead of using $\mathcal{R}(U)$ in Eq. (5.2), we can immediately write

$$U(t) = \mathcal{U}\left(I(t)\right). \tag{5.10}$$

The pump current induced by slow varying e.m.f. (5.9), can be easily found as the solution of Eq. (5.1) with small signal terms neglected. The inductive and resistive terms are negligible at low frequencies and we get for such a capacitance-dominated RCE

$$\mathcal{E}_{\mathrm{p}}(t) = \frac{1}{C_c} \int\limits_{-\infty}^{t} I_{\mathrm{p}}(t')\, dt', \tag{5.11}$$

which yields using Eq. (5.9):

$$I_{\mathrm{p}}(t) = -C_c \mu_0 S \ddot{H}_{\mathrm{p}}(t). \tag{5.12}$$

For a high frequency signal wave, all terms in Eq. (5.1) are important. Upon substituting the total current (5.3) in Eq. (5.10), expanding it with respect to weak signal contribution, we arrive at a particular form of Eq. (5.4):

$$U_\omega = \mathcal{R}(t) I_\omega, \tag{5.13}$$

where

$$\mathcal{R}(t) = \left. \frac{d\,\mathcal{U}(I)}{dI} \right|_{I=I_{\mathrm{p}}(t)} \tag{5.14}$$

stands for the effective insertion resistance, which follows changes of the pump current. The contour resistance R_c is negligible in comparison with that of the insertion. Then, Eq. (5.14) represents the total resistive part of the effective impedance (5.6) and determines the RCE quality factor. Accordingly, the dissipation in the metamaterial depends on pumping:

$$\Gamma = \frac{\omega_r^2}{\omega_0^2} \frac{1}{L_c} \mathcal{R}(t). \tag{5.15}$$

For an illustrative estimate of tuning range and required pump field values, we consider a circular RCE with radius $r_0 = 5\,\mathrm{mm}$ and wire diameter $1\,\mathrm{mm}$. Then the contour self-inductance equals $12\,\mathrm{nH}$ and an implemented capacitance of $0.23\,\mathrm{pF}$ ensures the resonant frequency $\omega_0 = 6\pi \cdot 10^9\,\mathrm{rad/s}$ ($\nu_0 = 3\,\mathrm{GHz}$) to be in the microwave frequency range. For the tetragonal arrangement of RCEs with lattice constants $b = 0.5\,r_0$ along the z-axis and $a = 2.1\,r_0$ in plane, the metamaterial resonance occurs at frequency $\omega_r \approx 3.6\pi \cdot 10^9\,\mathrm{rad/s}$ ($\nu_r \approx 1.8\,\mathrm{GHz}$).

Among variable resistance devices, backward diodes are prominent for relatively high sensitivity and reliable operation without additional bias. Taking, for example, InGaAs diodes reported by Schulman *et al.* (2001), with cross-section $10^3\,\mu\mathrm{m}^2$, we conclude that $\mathcal{U}(I)$ changes sufficiently at current values about 1 mA. To produce such a pump current, in accordance with Eq. (5.12), the values $\ddot{H} \sim 10^{19}\,\mathrm{A/ms}^2$ are required, which demands, for instance, fields of about $10^5\,\mathrm{A/m}$ with a characteristic varying time about $0.1\,\mu$s.

The assumed diode cross-section provides in the absence of pumping the resistance $R_0 = d\mathcal{U}/dI|_{I=0} = 23\,\Omega$; corresponding resonance width is $\Gamma_0 = 0.06\omega_r$ (RCE quality factor $Q_0 \approx 10$). Such medium has low absorption at frequencies $|\omega - \omega_r| \geq \Gamma_0$. Biasing the diode with appropriate $\ddot{H}$ one can achieve points on the current-voltage characteristic with higher $d\mathcal{U}/dI$. Clearly, already a 10 times increase yields $Q = 1$ and $\Gamma \sim \omega_r$, i.e., the absorption becomes substantial in a broad frequency band. Therefore, switching of the metamaterial between transparent and absorbing states in a wide frequency range is possible.

Remarkably, there exist points on the current-voltage characteristics of certain backward diodes, where $d\mathcal{U}/dI \to \infty$. Tuning the diode to such point would provide $Q \to \infty$, $\Gamma \to \infty$, which means that the medium becomes totally absorptive for signals at any frequency.

5.2.2 Variable capacitance

Varactors offer capacitance, dependent on the voltage drop on the element. We consider this dependence $\mathcal{C}(U)$ to be a known function. Generally, varactor resistance is also voltage dependent. However, the arising resistive contribution to the nonlinearity is much smaller than the capacitive one. Moreover, there are also varactors reported to have constant resistance [8]. Accordingly, we neglect the dependence for simplicity and consider Eq. (5.2) with constant $\mathcal{R}$:

$$U(t) = I(t)\mathcal{R} + \frac{1}{\mathcal{C}\left(U(t)\right)} \int\limits_{-\infty}^{t} I(t')\,dt'. \tag{5.16}$$

To maximize the resulting RCE nonlinearity, it is favourable to adjust the varactor capacitance $\mathcal{C}(0)$ so that no additional capacitance C_c is necessary to achieve the desired resonant frequency. Then Eq. (5.1) takes the form:

$$\mathcal{E}(t) = L_c\dot{I}(t) + U(t), \tag{5.17}$$

where we omit negligible resistance R_c of RCE conductor.

While determining slowly varying pump current and biasing voltage, we can disregard the inductive term in Eq. (5.17) as well as the resistive term in Eq. (5.16). Then, using Eq. (5.9), we get

$$U_{\mathrm{p}}(t) = -\mu_0 S \dot{H}_{\mathrm{p}}(t), \quad I_{\mathrm{p}}(t) = \frac{d}{dt}\Big[U_{\mathrm{p}}(t)\mathcal{C}\big(U_{\mathrm{p}}(t)\big)\Big]. \tag{5.18}$$

Next, we expand Eq. (5.16) with respect to small current and voltage at the signal frequency ω. Substituting in Eq. (5.17) and accounting for linear in U_ω, I_ω terms yields:

$$\mathcal{E}_\omega = \left[-i\omega L_c + \left(\mathcal{R} + \frac{i}{\omega C(t)}\right)\left(1 + U_{\mathrm{p}}(t)\frac{C'(t)}{C(t)}\right)^{-1}\right] I_\omega, \tag{5.19}$$

where

$$C(t) \equiv \mathcal{C}(U)\Big|_{U=U_{\mathrm{p}}(t)}, \qquad C'(t) \equiv \left.\frac{d\mathcal{C}(U)}{dU}\right|_{U=U_{\mathrm{p}}(t)} \tag{5.20}$$

are the pump-controlled functions of time.

The factor in square brackets in (5.19) represents the particular form of the effective RCE impedance (5.6). Correspondingly, we obtain the time dependent parameters of the permeability resonance:

$$\omega_0(t) = \Big(L_c\big[C(t) + U_{\mathrm{p}}(t)C'(t)\big]\Big)^{-1/2}, \tag{5.21}$$

$$\Gamma = \frac{\omega_r^2}{\omega_0^2}\frac{\mathcal{R}}{L_c}\left(1 + U_{\mathrm{p}}(t)\frac{C'(t)}{C(t)}\right)^{-1}. \tag{5.22}$$

The metamaterial resonant frequency is tuned proportionally to ω_0, and the resonance height A is not affected. Small variations of the resonant width are not valuable compared to the tuning of the metamaterial resonance. The latter determines the position of the metamaterial band gap, affecting critically the signals having frequencies close to the band gap edges and enables the transmission-reflection switching.

For qualitative estimates, we take typical examples of varactor diodes (Mamor *et al.*, 2001) and ferroelectric varactors (York *et al.*, 2001). To reach a remarkable tuning effect, the biasing voltage U_{p} should provide considerable changes of $\mathcal{C}(U)$. For varactor diodes, corresponding values of the biasing voltage are of the order of 0.5 V. Using Eq. (5.18), we obtain that $\dot{H}_{\mathrm{p}} \sim 5 \cdot 10^9$ A/m · s is required (for instance, an external field of about $5 \cdot 10^2$ A/m with a varying time about 0.1 μs). For ferroelectric varactors, the biasing voltage should be one order of magnitude higher, about 5 V, which enlarges the necessary pump field accordingly.

Note, that for tuning with slow fields varactor insertions demand field values of one or even two orders of magnitude lower than backward diodes.

There are two reasons for the robustness of backward diodes in the case considered. First, the requirement of the original metamaterial transparency demands the overall RCE reactance to be much larger than its resistance (the quality factor Q of at least 10). Therefore, the pump voltage drop on varactors is of the order of external electromotive force, while the voltage drop on backward diodes is much smaller. Second, the pump current (5.12) is proportional to the second time derivative of the external field, whereas the varactor pump current (5.18) involves the first derivative. With slow varying fields, this also decreases the resulting effectiveness of backward diodes.

5.3 Tuning by a high-frequency field

As follows from Eqs. (5.12), (5.18), in order to achieve substantial tuning using much lower pump magnetic field, one should decrease the characteristic varying times. The most convenient way to provide a fast varying magnetic field is to let a pump microwave propagate through the metamaterial. Choosing pump frequency Ω to lie in the transparency region below the metamaterial resonance, but still being comparable with the resonant frequency ω_r, one can also employ the resonant magnetization enhancement, which provides higher pump currents. As we show below, the high frequency regime allows decreasing the required pump field values by several orders of magnitude. Clearly, the adiabatic approximation of the Section 5.2 is no more valid and we develop a separate approach to describe this tuning regime.

In general, harmonic oscillating plane waves are not necessarily the eigenmodes of a highly nonlinear medium. To avoid this complication we concentrate on the case of weak RCE nonlinearity, although with the nonlinear insertions operating in highly nonlinear regime. Therefore, we have to ensure that the nonlinear contribution to U in Eq. (5.2) is small compared to linear in I terms in Eqs. (5.1), (5.2) at the pump frequency.

For the frequency Ω being comparable with the signal wave frequency ω, tuning can be accompanied by excitation of harmonics $\omega \pm l\Omega$ with any integer l. However, this is not relevant unless the phase matching conditions are specially met. Here we neglect the harmonics generation and concentrate on tuning.

Note that the macroscopic pump field in the bulk of the metamaterial differs from the externally applied field by a factor of the order of $\mu_{zz}(\Omega)$. The details of field distribution depend, especially for small samples, on particular sample shape and dimensions. However, if the sample is large enough, it is possible to obtain the pump wave with constant amplitude throughout the sample bulk. Thus, we assume the pump wave inside the metamaterial to have the z-component

$$H_z^{(\Omega)}(\mathbf{r},t) = H_\mathrm{p}\cos\left(\Omega t - \varphi(\mathbf{r})\right), \tag{5.23}$$

with homogeneous amplitude H_p and arbitrary phase φ changing at distances much larger than RCE size. Clearly, a plane running wave is a particular case of Eq. (5.23).

The amplitude of the pump current can be easily found from the magnetization of the medium at the pumping frequency, which has only one nonzero component $M_z = \aleph S I_\mathrm{p}$. Using the relation $M_z = (\mu_{zz} - 1)\, H_z$ between the magnetization and macroscopic magnetic field, we arrive at

$$I_\mathrm{p}(t) = I_0\cos\left(\Omega t - \varphi(\mathbf{r}_\mathrm{RCE})\right), \tag{5.24}$$

where the current amplitude is

$$I_0 = \left(\mu_{zz}(\Omega) - 1\right)\frac{H_\mathrm{p}}{\aleph S}, \tag{5.25}$$

and the phase is taken at the position $\mathbf{r}_\mathrm{RCE}$ of the RCE under consideration. Remarkably, it appears that the tuning effect is determined by the amplitude of I_p oscillation and is insensitive to its phase (see below). Therefore, the pump wave (5.23) produces homogeneous changes of the permeability.

Particular tuning effect of the pump current (5.24) is determined by the nonlinear insertion type and characteristics. Below we consider the cases of variable resistance and variable capacitance.

5.3.1 Variable resistance

As in previous, we consider the relation (5.10) for the voltage drop on the insertion. The current in RCE is given by Eq. (5.3) with pumping term Eq. (5.24). Substitution in Eq. (5.1) and expansion with respect to small I_ω yields

$$\mathcal{E}_\omega = \left[-i\omega L_c + \frac{i}{\omega C_c} + R(I_0)\right] I_\omega, \tag{5.26}$$

where we can neglect ohmic losses in the RCE conductor, and rewrite the overall RCE resistance as

$$R(I_0) = \left\langle \left.\frac{d\mathfrak{U}(I)}{dI}\right|_{I=I_0\cos(\Omega t-\varphi)} \right\rangle. \tag{5.27}$$

The involved zero Fourier component of the oscillating instantaneous resistance is equivalent to the value, averaged over period $2\pi/\Omega$; it is denoted here by $\langle \ldots \rangle$-brackets. The averaged value depends neither on Ω nor on φ, which ensures the homogeneous tuning by a running wave.

As seen from Eq. (5.26), the pumping affects the effective resistance of RCE. This finally results in tuning of the metamaterial resonance width:

$$\Gamma(H_{\mathrm{p}}, \Omega) = \frac{\omega_r^2}{\omega_0^2} \frac{1}{L_c} R(I_0), \tag{5.28}$$

which appears to be dependent via I_0 on the pump field amplitude and frequency (see Eq. (5.25)).

To estimate the arising tuning capabilities with backward diodes (Schulman *et al.*, 2001) we model typical current-voltage characteristics (Fig. 5.1a), assuming feasible diode cross-section $10^3\,\mu\mathrm{m}^2$. Corresponding relative resistance changes $R(I_0)/R(0)$ are shown in Fig. 5.1b. For some of the modeled characteristics, the effective resistance demonstrates a remarkable peak. It is easy to explain the origin of this sharp peak: it occurs when the pump current amplitude matches the local maximum of the current-voltage characteristic, where $d\mathcal{U}/dI$ tends to infinity. Corresponding contribution to the averaged value (5.27) increases drastically then, since the diode spends considerable time interval in the vicinity of this critical point.

We conclude that for the modeled diodes, the effective RCE resistance can be increased by up to one order of magnitude. This requires the amplitude of the pump current about 1 mA. Using Eq. (5.25) with the chosen metamaterial parameters (see Section 5.2.1) we estimate the pump field amplitude of the order of 0.3 A/m to be sufficient. Comparing with the estimates in Section 5.2.1 shows that the high-frequency tuning indeed demands much lower field amplitudes. On the other hand, achievable Γ modulation is smaller.

5.3.2 Variable capacitance

We consider, like in Section 5.2.2, an RCE with the capacitance being provided by a varactor insertion. The pump voltage drop on the varactor can be obtained from Eq. (5.16) for the known pump current (5.24). At this step, we can neglect the weak signal contribution as well as the small resistance in (5.16). Then the pump voltage obeys the transcendental equation

$$U_{\mathrm{p}}(t)\mathcal{C}\big(U_{\mathrm{p}}(t)\big) = \frac{1}{\Omega} I_{\mathrm{p}}(t). \tag{5.29}$$

Obviously, $U_{\mathrm{p}}(t)$ is a $2\pi/\Omega$ periodic function; it can be obtained from this equation for a particular varactor with known $\mathcal{C}(U)$.

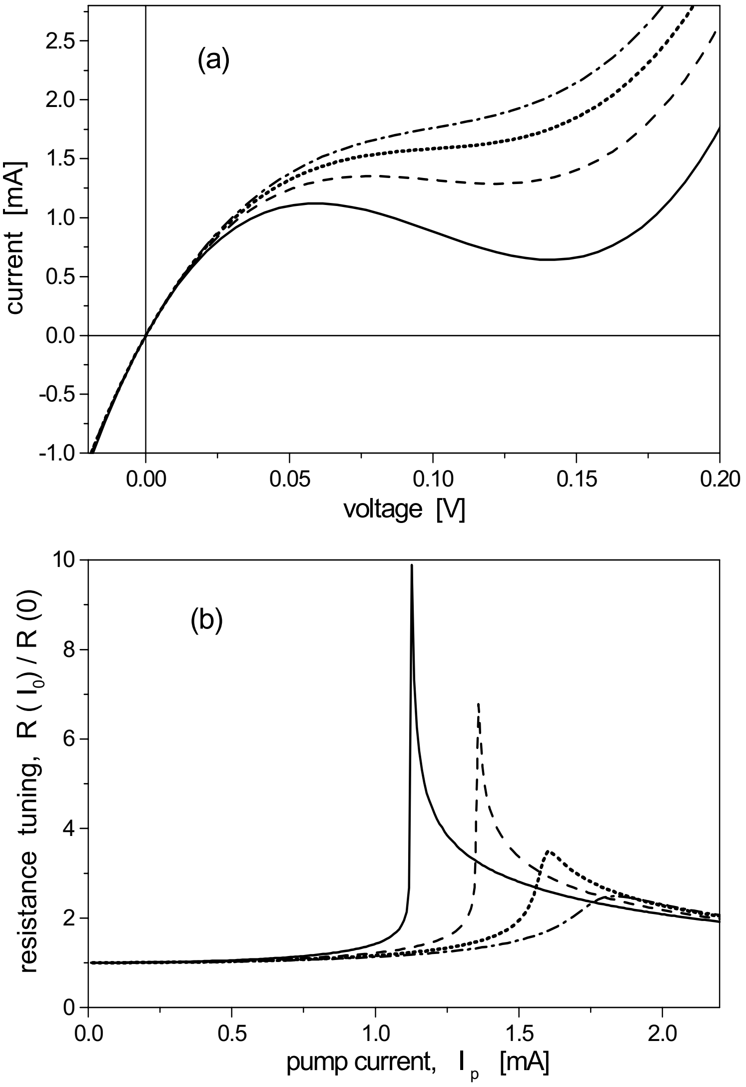

Figure 5.1: Resistance tuning with backward diodes. (a) Model current-voltage characteristics of backward diodes. (b) Corresponding dependances of the relative resistance change on pump current.

Next, we substitute the voltage drop (5.3) into Eqs. (5.16), (5.17), and expand them with respect to the signal voltage U_ω, obtaining:

$$\mathcal{E}_\omega = \left[-i\omega L_c + \left(\mathcal{R} + \frac{i}{\omega} \left\langle \frac{1}{C(t)} \right\rangle \right) \left(1 + \left\langle U_\mathrm{p}(t) \frac{C'(t)}{C(t)} \right\rangle \right)^{-1} \right] I_\omega, \qquad (5.30)$$

where $C(t)$ and $C'(t)$ are defined by (5.20).

Note, that Eq. (5.30) resembles Eq. (5.19) with an important distinction that the averaging over the period $2\pi/\Omega$ is performed. Taking Eq. (5.29) into account, it is easy to obtain that the averaged values are controlled by pumping via parameter $g = I_0/\Omega$. Accordingly, the RCE resonant frequency and the metamaterial resonance width are g-dependent:

$$\omega_0(g) = \left\langle \frac{1}{C(t)} \right\rangle^{1/2} \left(L_c \left(1 + \left\langle U_\mathrm{p}(t) \frac{C'(t)}{C(t)} \right\rangle \right) \right)^{-1/2}, \qquad (5.31)$$

$$\Gamma = \frac{\omega_r^2}{\omega_0^2} \frac{\mathcal{R}}{L_c} \left(1 + \left\langle U_\mathrm{p}(t) \frac{C'(t)}{C(t)} \right\rangle \right)^{-1}. \qquad (5.32)$$

The shift of the metamaterial resonant frequency ω_r is proportional to the shift (5.31) of ω_0. The resonance height A remains constant.

We remind that in order to deal with harmonic pump wave, we have to ensure that it is only slightly distorted by nonlinear insertion influence. Therefore, the pump-induced modulation of the effective RCE capacitance should not be strong. This means, in particular, that the parameters (5.31), (5.32) should not be altered significantly by pumping, i.e., $|\omega_0(g) - \omega_0(0)| \ll \omega_0(0)$ and $|\Gamma(g) - \Gamma(0)| \ll \Gamma(0)$. Such changes of the resonance width are hardly observable, whereas the resonance shift affects crucially propagation of signal waves with frequencies close to ω_r.

For illustrative estimates, we model characteristic dependencies $\mathcal{C}(U)$ for varactor diodes (Mamor *et al.*, 2001) and ferroelectric varactors (York *et al.*, 2001) as shown in Fig. 5.2a and Fig. 5.3a, respectively. We calculate the corresponding relative shift of the resonance $\omega_r(g)/\omega_r(0)$, taking RCE and metamaterial parameters as in Section 5.2.1. Fig. 5.2b and Fig. 5.3b show that tuning of the resonant frequency by 10% is achievable with $g \sim 5 \cdot 10^{-14}\,\mathrm{A \cdot s}$ for the modeled varactor diodes and $g \sim 5 \cdot 10^{-14}\,\mathrm{A \cdot s}$ for the ferroelectric varactors. In accordance with Eq. (5.25), corresponding pump field amplitudes are $H_\mathrm{p} \sim 0.1\,\mathrm{A/m}$ and $H_\mathrm{p} \sim 0.5\,\mathrm{A/m}$.

Comparing the estimations for the high frequency tuning, we see that the pump field amplitudes required for remarkable tuning are of the same order for backward diodes and varactors. As expected, these field amplitudes are several orders of magnitude lower than those for the slow-field tuning. This makes the high frequency tuning much more attractive for practice.

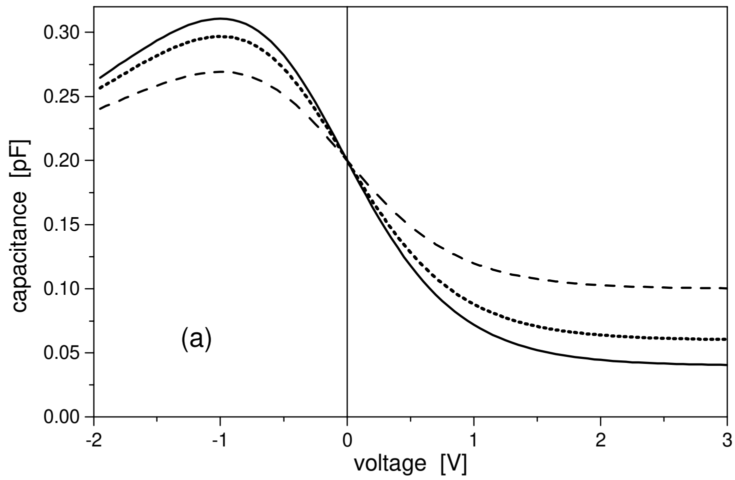

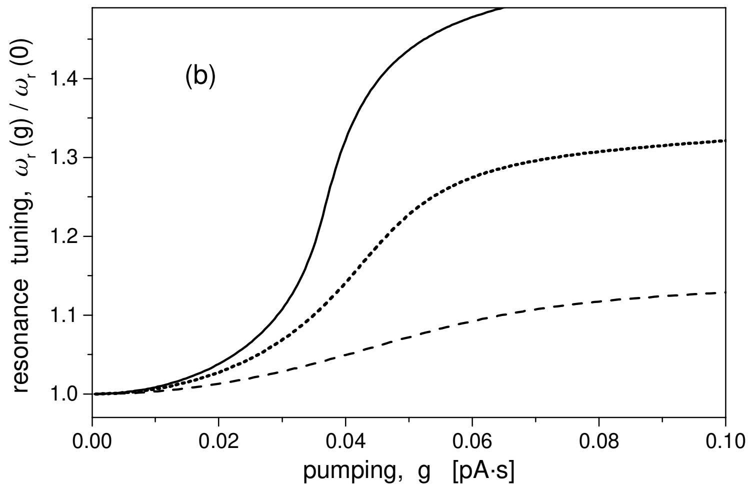

Figure 5.2: Resonance tuning with varactor diodes. (a) Model capacitance-voltage characteristics of varactor diodes. (b) Corresponding dependances of the relative resonance shift on pumping parameter g.

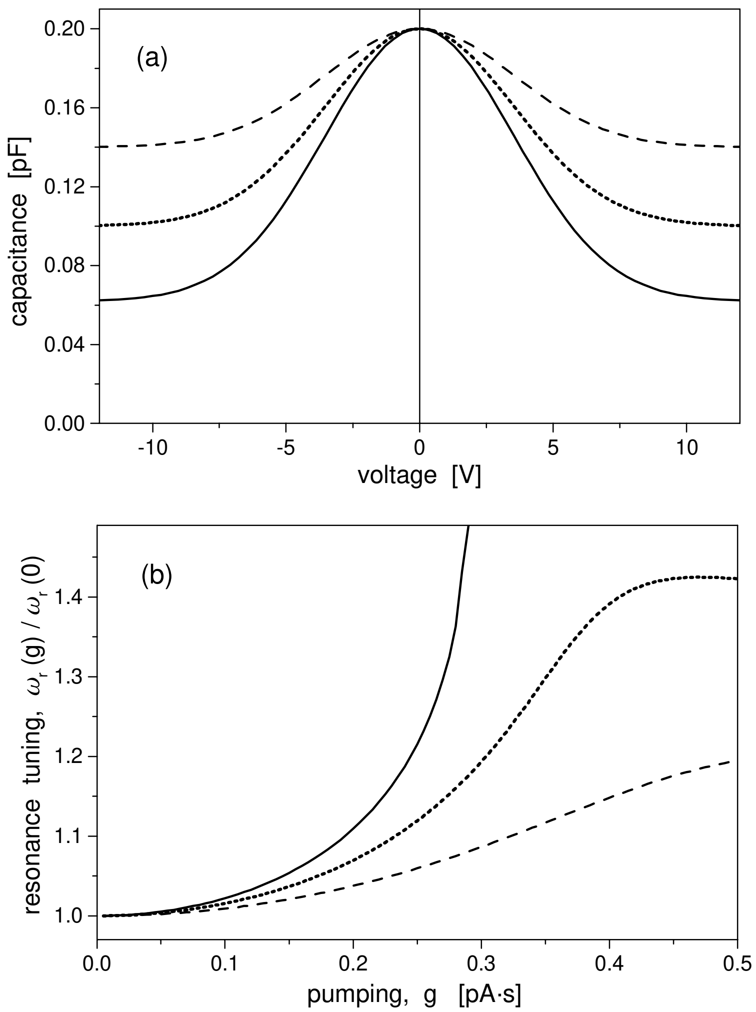

Figure 5.3: Resonance tuning with ferroelectric varactors. (a) Model capacitance-voltage characteristics of ferroelectric varactors. (b) Corresponding dependances of the relative resonance shift on pumping parameter g.

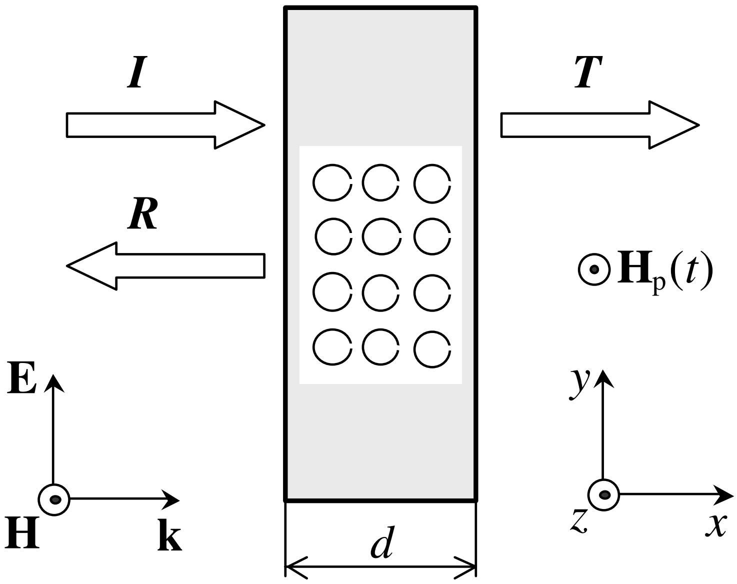

Figure 5.4: Transmission-reflection setup for metamaterial slab. Orientation of RCEs is schematically shown.

5.4 Tuned band gap of a metamaterial slab

To get a better insight into the application capabilities of the metamaterial tuning, we turn to a simple example and study a transmission-reflection problem for a metamaterial slab with tunable permeability. Schematic of the problem is presented in Fig. 5.4. Since the metamaterial interacts only with the z-component of magnetic field, we choose the corresponding polarization of the incident (I) signal wave. For simplicity, we disregard the interaction of RCEs with the electric field (which is weak relative to the resonant magnetic interaction) and assume the permittivity to be given by a unit tensor: $\varepsilon_{ij} = \delta_{ij}$. The chosen coordinate axes are the principal axes of both permeability and permittivity tensors and therefore transmitted (T) and reflected (R) waves are polarized in the same way as the incident wave.

For a normal incidence of the signal wave, the slab transmittance T and reflectance F take the form (Landau and Lifschitz, 1984):

$$T = \frac{\left|4\Psi\sqrt{\mu_{zz}(\omega)}\right|^2}{\left|\Psi^2\left(1-\sqrt{\mu_{zz}(\omega)}\right)^2 - \left(1+\sqrt{\mu_{zz}(\omega)}\right)^2\right|^2}, \tag{5.33}$$

$$F = \frac{\left|\left(1-\Psi^2\right)\left(1-\mu_{zz}(\omega)\right)\right|^2}{\left|\Psi^2\left(1-\sqrt{\mu_{zz}(\omega)}\right)^2-\left(1+\sqrt{\mu_{zz}(\omega)}\right)^2\right|^2}, \tag{5.34}$$

where $\Psi = \exp\left(i\omega c^{-1} d\sqrt{\mu_{zz}(\omega)}\right)$.

Note that the transmittance and reflectance are controlled by only two parameters: the slab thickness d and permeability μ_{zz}. We distinguish between three qualitatively different states:

- transmitting slab, with $T \approx 1$, $F \ll 1$;
- reflecting slab, with $T \ll 1$, $F \approx 1$;
- absorbing slab, with $T \ll 1$, $F \ll 1$.

Adjusting the permeability by external magnetic field one can vary the coefficients (5.33), (5.34) and switch the slab between these three states.

It appears that a slab thickness comparable with the microwave wavelength in vacuum, $\lambda_0 = 2\pi c/\omega_0$, is large enough for substantial transmittance modulation. Setting the thickness $d = \lambda_0$, we concentrate on the

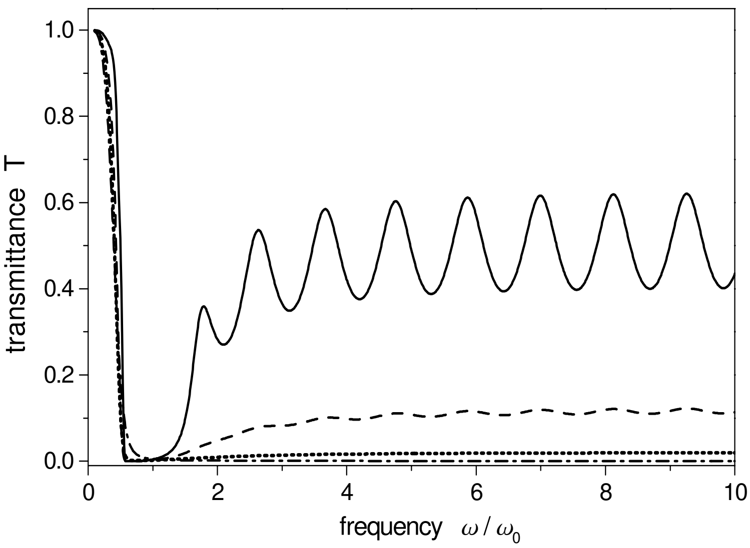

Figure 5.5: Transmittance of metamaterial slab in a broad frequency range with the RCE quality factor $Q = 10$ (solid line), 2 (dashed line), 1 (dotted line), and 0.5 (dash-dot line).

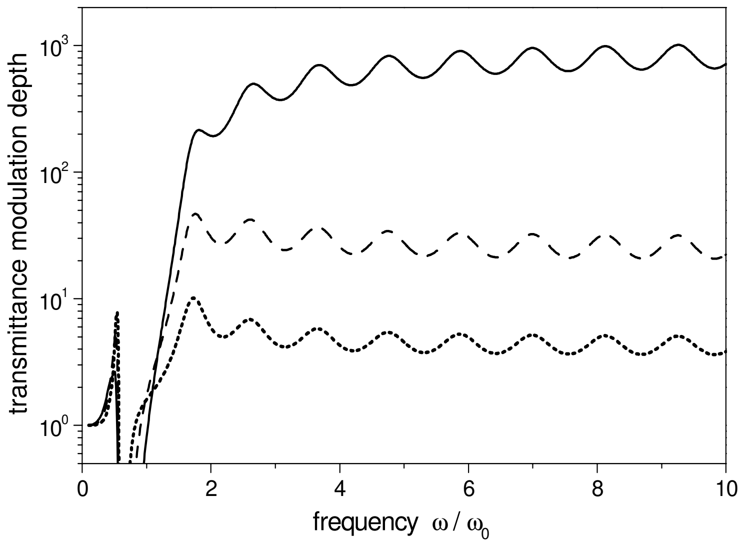

Figure 5.6: Relative change of slab transmittance for the 5-fold (dotted line), 10-fold (dashed line), and 20-fold (solid line) decrease of the RCE quality factor.

transmission coefficient T as a function of the signal frequency ω and study the changes caused by the pumping.

Variable resistance insertions allow controlling the RCE quality factor and, as a consequence, the metamaterial resonance width. We have demonstrated that for both considered types of tuning (slow and high frequency pumping) a 5-10 fold decrease of the quality factor is achievable. Resulting changes in the transmittance are presented in Fig. 5.5. Taking the RCE quality factor $Q = 10$ in the absence of pumping ensures that the slab is initially transparent ($T \sim 0.5$) in a wide frequency range above the band gap. We characterize the tuning efficiency with the transmittance modulation depth (ratio of the untuned to tuned transmittance). Fig. 5.6 shows that 5-fold decrease of the quality factor leads to noticeable absorption of the signal wave resulting in a 5-fold decrease of the transmittance. A 10-fold decrease of the quality factor lowers the transmitted signal intensity by about 30 times. A 20-fold decrease of the quality factor practically blocks the transmission. Such an extreme modulation is apparently not feasible with the high frequency tuning, but can be realized with the slow tuning regime.

Variable capacitance insertions provide a possibility to tune the metamaterial resonance and, consequently, to shift the band gap. With both regimes of tuning, the resonant frequency can be altered by up to 30% and more.

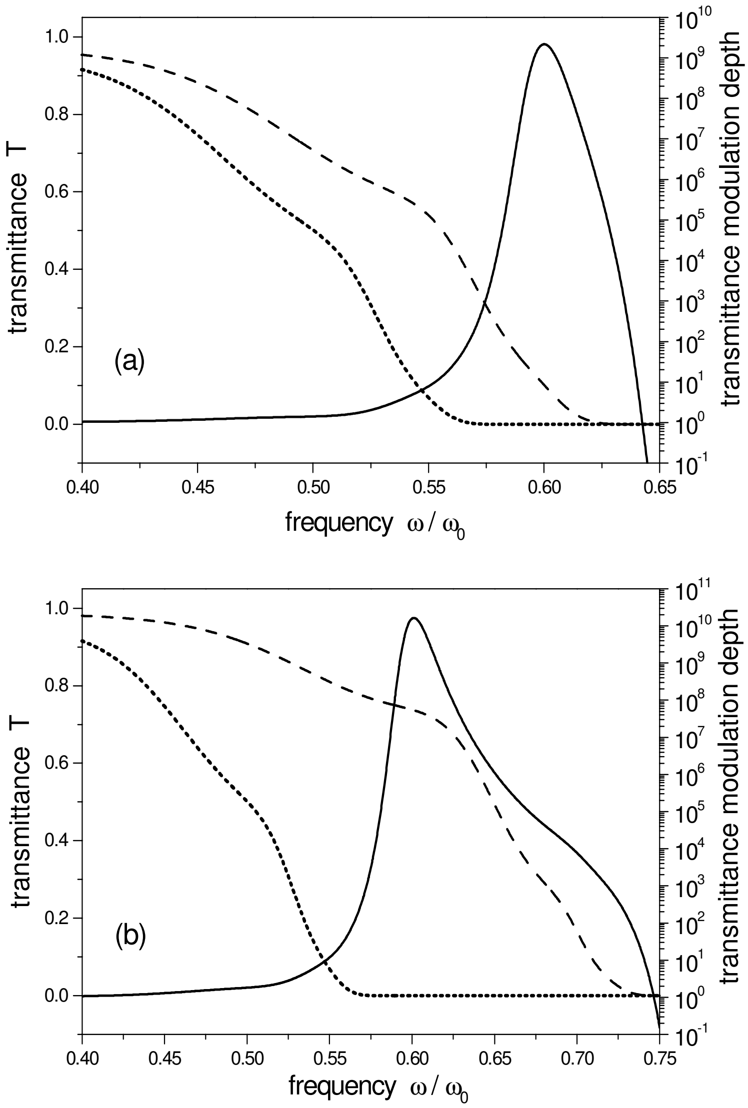

Figure 5.7: Tuning of the metamaterial slab transmittance with 10% (a) and 30% (b) shift of the band gap. Transmittances of the non-tuned slab (dotted line), of the slab with shifted resonance (dashed line), and resulting transmission modulation (solid line) are shown.

In Fig. 5.7 we show two examples of corresponding changes in the transmittance. Shifting the band gap by 10% allows varying the transmittance by up to nine orders of magnitude in a narrow frequency range between the original and shifted band gap edges (see Fig. 5.7a). However, the transmittance at such frequencies remains below 0.2, i.e., the most part of the incident power is absorbed or reflected anyway. Switching to a state with higher transmittance becomes possible if the shift of the resonance exceeds the width of the transition region near the band gap edge. Thus, a 30% resonance shift makes it possible to modulate the transmittance between 0.8 and practically zero.

5.5 Discussion

In this chapter we have analyzed the possibility to tune the linear electromagnetic properties of nonlinear metamaterial with external varying magnetic field. We have shown that the variable resistance insertions provide an opportunity to tune the width of the metamaterial resonance and, accordingly, to control the medium absorbance. Variable capacitance insertions allow shifting the metamaterial magnetic resonance, which determines the band gap.

Slow-field tuning regime allows broad variation of the metamaterial properties but requires extremely high values of external field. The high-frequency tuning by a pump microwave appears to demand much lower fields and we conclude it to be the most promising for applications.

Relying on the estimates, performed for backward diodes, varactor diodes, and ferroelectric varactors, employed as nonlinear insertions, we conclude that the high frequency tuning requires the amplitude of magnetic field in pump wave to be of the order of 0.1 A/m, which appears to be quite feasible.

We demonstrated that variable resistance insertions enable a broad-band transmittance modulation by 1–2 orders of magnitude, whereas variable capacitance insertions provide a narrow-band modulation by several orders of magnitude. Such effects can be achieved using a relatively thin slab of metamaterial, having the thickness comparable with a microwave wavelength.

The reported metamaterial tunability is analogous to electro-optic effect, known for more than a century and widely exploited nowadays in optic technology. We expect, therefore, that tunable nonlinear metamaterials will become key elements of innovative microwave devices for an optic-like manipulation with microwaves.

Chapter 6

Summary and outlook

In summary, in the frame of work on this thesis, we have

- developed the theory of linear magnetic response of RCE-metamaterials (Chapter 2);
- considered the possibility to create a magnetically nonlinear metamaterial and analyzed the nonlinear properties in the limit of weak nonlinearity (Chapter 3);
- introduced an approach for describing microwave coupling in metamaterials at high nonlinearity, taking three-wave coupling as an example (Chapter 4);
- proposed tunable metamaterials with controllable band gap for microwaves and discussed the details and efficiency of tuning (Chapter 5).

Following the classical methods of the electrodynamics of condensed matter, we have shown, how the macroscopic parameters of metamaterial can be calculated, and how they depend on the characteristics of structure elements and the details of their arrangement. We analyzed frequency dispersion of the effective permeability and pointed out that the mutual interaction of the elements affect significantly frequency and width of the resonance. In particular, we demonstrated how to optimize the metamaterial parameters for dealing with negative refraction phenomenon.

In addition, we performed *ab initio* numerical simulation of a finite sample of metamaterial, which yielded complete agreement with the analytical approach, and proved that for a very precise numerical permeability calculation it is sufficient to study a relatively small sample, instead of huge numerics, often seen in literature (e.g. Weiland *et al.*, 2001).

Continuing to ensue the analogy to crystals, we have shown that the metamaterial with nonlinear insertions can host immediate microwave interaction. The wave coupling can be described via quadratic nonlinear susceptibility, as long as the wave fields' amplitude is low, so that the insertions operate in the vicinity of zero bias. Even for this limit, however, we estimated that a nonlinear modulation of magnetic susceptibility of the order of 0.001 can be reached in practice, being much higher than ever observed in optics. The only disadvantage, encountered in this case, is relatively large energy dissipation, which narrows down application possibilities.

Having turned to higher wave intensities, when the universal "optical" approach is no longer valid, we analyzed two quite representative nonlinear phenomena: three-wave interaction and band gap tuning. Concerning the first one, we worked out the method, which enables to calculate coupling parameters for a given characteristic of insertions. It appears that the coupling strength depends nonlinearly on the pump field amplitude, and that the general appearance of this dependence differs remarkably, whether variable resistance or variable capacitance is employed. We estimate that exceptionally high nonlinear modulation — of the order of 0.1 — can be reached using typical devices reported in current literature.

We should note that extreme strength of nonlinear coupling is indeed of higher demand for metamaterials, than for optics, because it decreases required interaction length. In contrast to crystals, where very long (compared to wavelengths) interaction distances are normally available, for metamaterials relatively small dimensions become relevant due to a much larger scale.

Concerning the tunability of metamaterials, we proposed two tuning regimes, exploiting either slowly varying external magnetic field, or strong pump microwave. We demonstrate that depending on the type of nonlinearity, both regimes allow controlling the resonance width and the resonance frequency of the permeability. Accordingly, the metamaterial can be switched between transparent, reflecting or absorbing states with respect to propagating microwaves. For an illustration of tuning capabilities, we have shown that rather thin slab of metamaterial (with thickness of the order of one wavelength) is suitable for very efficient band gap tuning.

The properties and distinctions of metamaterials, considered in this thesis, represent important basics and imply valuable applications. On the other hand, the range of interesting and promising phenomena is far from being exhausted. For example, peculiar behaviour of metastructure at frequencies, close to resonance (see section 2.4), is concerned with evoking exitons and standing waves. These are in close connection with the magnetoinductive waves, which are the subject of fruitful research by E. Shamonina and coworkers (Shamonina and Solymar, 2004; Wiltshire *et al.*, 2004).

We would like to suggest at least some of directions for further investigation, which arise from the presented results and conclusions.

- In sections 4.2.2 and 4.3.2 we have seen that in certain cases the nonlinear contribution tends to exceed magnitudes, acceptable within the frame of presented approach. In this situation, harmonic waves are not the eigenmodes of medium any longer, and a special treatment is necessary. Such an extreme nonlinearity might offer unusual applications and is worth studying.

- Although Chapter 4 refers particularly to three-wave interaction with one pump wave, the reported method provides a ground for developing a description for other coupling processes, e.g., with two or three strong waves, as well as various four-wave interactions.

- Besides the two tuning regimes, proposed in Chapter 5, one can check other solutions, for instance, employing electric fields at extra high frequencies, as suggested by Tretyakov (2004).

- Along with the tunability of the linear properties, which itself leaves a bundle of details to continue with, we should point at an exclusive possibility to tune the nonlinear response, as it was mentioned in section 4.3.2. Analyzis and optimizing of such tuning are likely to bring valuable outcome.

Furthermore, the estimates, reported in this thesis, are merely illustrative; particular experiments would offer possibility for farther optimization.

We believe that a number of useful and surprising features awaits a researcher, who chases in the field of metamaterials.

Bibliography

Abadei, S., S. Gevorgian, C.-R. Cho and A. Grishin (2002). Low-frequency and microwave performances of laser-ablated epitaxial $Na_{0.5}K_{0.5}NbO_3$ films on high-resistivity SiO_2/Si substrates. *Journal of Applied Physics* **91**, 2267.

Agranovich, V. M. and V. L. Ginzburg (1967). *Spatial Dispersion in Crystal Optics and the Theory of Excitons*. Wiley, New-York.

Agranovich, V. M., Y. R. Shen, R. H. Baughman and A. A. Zakhidov (2004). Linear and nonlinear wave propagation in negative refraction metamaterials. *Physical Review B* **69**, 165112.

Bayindir, M., K. Aydin, E. Ozbay, P. Markoš *et al.* (2002). Transmission properties of composite metamaterials in free space. *Applied Physics Letters* **81**(1), 120.

Bloembergen, N. (1965). *Nonlinear Optics*. Benjamin, New-York.

Canedy, C. L., H. Li, S. P. Alpay, L. Salamanca-Riba *et al.* (2001). Dielectric properties in heteroepitaxial $Ba_{0.6}Sr_{0.4}TiO_3$ thin films: Effect of internal stresses and dislocation-type defects. *Applied Physics Letters* **78**(16), 2354.

Cho, C.-R., J.-H. Koh, A. Grishin, S. Abadei *et al.* (2002). $Na_{0.5}K_{0.5}NbO_3/SiO_2$/Si thin film varactor. *Journal of Applied Physics* **91**, 2267.

Fu, Y., M. Mamor, M. Willander, S. Bengtsson *et al.* (2000). n-Si/SiO_2/Si heterostructure barrier varactor diode design. *Applied Physics Letters* **77**(1), 103.

Gay-Balmaz, P. and O. J. F. Martin (2002). Electromagnetic resonances in individual and coupled split-ring resonators. *Journal of Applied Physics* **92**(5), 2929.

Gorkunov, M., M. Lapine, E. Shamonina and K. H. Ringhofer (2002). Effective magnetic properties of a composite material with circular conductive elements. *European Physical Journal B* **28**, 263.

Gorkunov, M. V. and M. I. Ryazanov (1997). *Sov. Journal of Experimental and Theoretical Physics* **85**, 97.

Grbic, A. and G. V. Eleftheriades (2002). Experimental verification of backward-wave radiation from a negative refractive index metamaterial. *Journal of Applied Physics* **92**(10), 5930.

Helszajn, J. (1978). *Passive and Active Microwave Circuits*. Wiley, New-York.

Ivanov, S. N., N. A. Penin, N. E. Skvortsova and Y. F. Sokolov (1969). *Physics of Microwave Semiconductor Diodes*. Iliffe Books LTD, London.

Jackson, J. D. (1999). *Classical Electrodynamics*. Wiley, New-York.

Kalinin, V. A. and V. V. Shtykov (1991). On the Possibility of Reversing the Front of Radio Waves in an Artificial Nonlinear Medium. *Journal of Communications Technology and Electronics* **36**, 96. Originally in Radiotekhnika i Elektronika, No. 11, 2275–2281 (1990).

Kollberg, E. L., J. Stake and L. Dillner (1996). Heterostructure barrier varactors at submillimetre waves. *Phil. Trans. R. Soc. Lond. A* **354**, 2383.

Kostin, M. V. and V. V. Shevchenko (1993). Theory of Artificial Magnetic Substances Based on Ring Currents. *Journal of Communications Technology and Electronics* **38**(5), 72. Originally in Radiotekhnika i Elektronika, No. 11, 1992–2003 (1992).

Kozyrev, A., A. Ivanov, T. Samoilova, O. Soldatenkov *et al.* (2000). Nonlinear response and power handling capability of ferroelectric $Ba_xSr_{1-x}TiO_3$ film capacitors and tunable microwave devices. *Journal of Applied Physics* **88**(9), 5334.

Landau, L. D. and E. M. Lifschitz (1984). *Electrodynamics of Continuous Media*. Pergamon Press, Oxford.

Lapine, M., M. Gorkunov and K. H. Ringhofer (2003). Nonlinearity of a metamaterial arising from diode insertions into resonant conductive elements. *Physical Review E* **67**, 065601(R).

Lebedev, I. V. and M. Y. Polyakov (2000). Frequency Characteristics of Stepwise Varactor Structures. *Journal of Communications Technology and Electronics* **46**(4), 463. Translated from Radiotekhnika i Elektronika, **46**(4), 498 (2001).

Li, H., A. L. Roytburd, S. P. Alpay, T. D. Tran *et al.* (2001). Dependence of dielectric properties on internal stresses in epitaxial barium strontium titanate thin films. *Applied Physics Letters* **78**(16), 2354.

Lindell, I. V., S. A. Tretyakov, K. I. Nikoskinen and S. Ilvonen (2001). BW media — media with negative parameters, capable of supporting backward waves. *Microwave and Optical Technology Letters* **31**(2), 129.

Mamor, M., Y. Fu, O. Nur, M. Willander *et al.* (2001). Leakage current and capacitance characteristics of Si/SiO_2/Si single-barrier varactor. *Applied Physics A* **72**, 633.

Marqués, R., J. Martel, F. Mesa and F. Medina (2002a). Left-Handed-Media Simulation and Transmission of EM Waves in Subwavelength Split-Ring-Resonator-Loaded Metallic Waveguides. *Physical Review Letters* **89**(18), 183901.

Marqués, R., F. Medina and R. Rafii-El-Idrissi (2002b). Role of bianisotropy in negative permeability and left-handed metamaterials. *Physical Review B* **65**, 144440.

Marso, M., M. Wolter, P. Javorka, A. Fox *et al.* (2001). AlGaN/GaN varactor diode for integration in HEMT circuits. *Electronics Letters* **37**(24), 1476.

O'Brien, S., D. McPeake, S. A. Ramakrishna and J. B. Pendry (2004). Near-infrared photonic band gaps and nonlinear effects in negative magnetic metamaterials. *Physical Review B* **69**, 241101(R).

Pendry, J. B. (2001). Electromagnetic materials enter the negative age. *Physics World* **14**(9), 47.

Pendry, J. B., A. J. Holden, D. J. Robbins and W. J. Stewart (1999). Magnetism from Conductors and Enhanced Nonlinear Phenomena. *IEEE Trans. Microwave Theory Tech.* **47**, 2075.

Razumov, S. V., A. V. Tumarkin, A. G. Gagarin, M. V. Sysa *et al.* (2003). Microwave Properties of Thin BSTO Films Based Varactors for High Frequency Applications. *Integrated Ferroelectrics* **55**, 871.

Reynet, O. and O. Acher (2004). Voltage controlled metamaterial. *Applied Physics Letters* **84**, 1198.

Ryazanov, M. I. (1984). *Condensed Matter Electrodynamics*. Nauka, Moscow.

Ryazanov, M. I. (1995). *Sov. Journal of Experimental and Theoretical Physics* **81**, 974.

Schubert, M. and B. Wilhelmi (1971). *Einführung in die nichtlineare Optik*. Teubner, Leipzig.

Schulman, J. N., D. H. Chow and D. M. Jang (2001). Ingaas Zero Bias Backward Diodes for Millimeter Wave Direct Detection. *IEEE Electron Device Letters* **22**, 200.

Shamonin, M., E. Shamonina, V. Kalinin and L. Solymar (2004). Properties of a metamaterial element: Analytical solutions and numerical simulations for a singly split double ring. *Journal of Applied Physics* **95**(7), 3778.

Shamonina, E., V. A. Kalinin, K. H. Ringhofer and L. Solymar (2001). Magneto-inductive waveguide. *Electronic Letters* **37**, 1243.

Shamonina, E., V. A. Kalinin, K. H. Ringhofer and L. Solymar (2002a). Magnetoinductive waves in one, two, and three dimensions. *Journal of Applied Physics* **92**, 6252.

Shamonina, E., M. Lapine, K. H. Ringhofer and L. Solymar (2002b). In *Proceedings of the Progress in Electromagnetics Research Symposium*, 249. (July 2002, Cambridge, MA, USA).

Shamonina, E. and L. Solymar (2004). Magneto-inductive waves supported by metamaterial elements: components for a one-dimensional waveguide. *Journal of Physics D: Applied Physics* **37**, 362.

Shelby, R. A., D. R. Smith, S. C. Nemat-Nasser and S. Schultz (2001a). Microwave transmission through a two-dimensional, isotropic, left-handed metamaterial. *Applied Physics Letters* **78**, 489.

Shelby, R. A., D. R. Smith and S. Schultz (2001b). Experimental verification of a negative index of refraction. *Science* **292**, 77.

Smith, D. R., W. J. Padilla, D. C. Vier, S. C. Nemat-Nasser *et al.* (2000a). Composite Medium with Simultaneously Negative Permeability and Permittivity. *Physical Review Letters* **84**, 4184.

Smith, D. R., S. Schultz, P. Markoš and C. M. Soukoulis (2002). Determination of effective permittivity and permeability of metamaterials from reflection and transmission coefficients. *Physical Review B* **65**, 195104.

Smith, D. R., D. C. Vier, N. Kroll and S. Schultz (2000b). Direct calculation of permeability and permittivity for a left-handed metamaterial. *Applied Physics Letters* **77**(14), 2246.

Sze, S. M. (1981). *Physics of Semiconductor Devices*. Wiley, New-York.

Tappe, S., U. Böttger and R. Waser (2003). Investigation of the High Frequency Properties of BST Thin Films — A Comparison of Three Different Commonly Used Methods. *Integrated Ferroelectrics* **53**, 455.

Tretyakov, S. A. (2001). Meta-materials with wideband negative permittivity and permeability. *Microwave and Optical Technology Letters* **31**(3), 163.

Tretyakov, S. A. (2004). Personal communication.

Vanbésien, O., G. Beaudin and J. C. Pernot (1999). III-V devices for application at millimeter and submillimeter wavelengths. *Journal de Physique IV France* **9**, 151.

Veselago, V. G. (1968). The electrodynamics of substances with simultaneously negative values of ϵ and μ. *Soviet Physics Uspekhi* **10**(4), 509. Translated from Usp. Fiz. Nauk **92**, 517 (1967).

Weiland, T., R. Schuhmann, R. B. Greegor, C. G. Parazzoli *et al.* (2001). *Ab initio* numerical simulation of left-handed metamaterials: Comparison of calculations and experiments. *Journal of Applied Physics* **90**(10), 5419.

Wiltshire, M. C. K., E. Shamonina, I. R. Young and L. Solymar (2004). Experimental and theoretical study of magneto-inductive waves supported by one-dimensional arrays of "swiss rolls". *Journal of Applied Physics* **95**(8), 4488.

York, R. A., A. S. Nagra, P. Periaswamy, O. Auciello *et al.* (2001). Synthesis and Characterization of $(Ba_xSr_{1-x})Ti_{1+y}O_{3+z}$ Thin Films and Integration into Microwave Varactors and Phase Shifters. *Integrated Ferroelectrics* **34**, 177.

Zharov, A. A., I. V. Shadrivov and Y. S. Kivshar (2003). Nonlinear properties of left-handed metamaterials. *Physical Review Letters* **91**, 037401.

Ziolkowski, R. W. (2001). Superluminal transmission of information through an electromagnetic metamaterial. *Physical Review E* **63**, 046604.

Acknowledgements

My deepest gratitude is to Professor Klaus Ringhofer, my initial scientific advisor, who guided me through the first steps towards my entity in physics, and who has created a working group so effective and cheerful that it was an honour for me to belong to.

I am exceptionally grateful to Prof. Klaus Betzler and to Dr. Maxim Gorkounov for their readiness to adopt the supervising role and for their care and reliable support of my further research progress.

I would not have started this PhD project in physics without Dr. Ekaterina Shamonina, who introduced me to the Theoretical Optics group, helped tremendously to start my activity in a novel and interesting research field of metamaterials, and remains to be a reliable, attentive and willing advisor.

It is impossible to overestimate the role of my immediate scientific advisor, Dr. Maxim Gorkunov, who opened the world of theoretician to me. His deep scientific experience, responsive and skillful guidance enabled me to participate in world-class research and to accomplish a thesis in a rapidly developing and promising branch of modern electrodynamics.

I am very grateful to the chairs of the Graduate College 695, Prof. Dr. E. Krätzig and Prof. Dr. K. Betzler, who masterfully maintained the College at the excellent level of organization and were ready to help with any problems occurred.

It was my great pleasure to start with my first tasks in close collaboration with Prof. Laszlo Solymar and Dr. Ekaterina Shamonina, whose great enthusiasm and tact give an example in these days.

I would like to express my appreciation to Prof. Boris Sturman, who have been always open for discussions and provided me with a lot of valuable advice.

The courses of lectures offered by Prof. Dr. K. H. Ringhofer, Prof. Dr. E. Krätzig, Dr. E. Shamonina, Prof. Dr. P. Hertel, Prof. Dr. H.-J. Schmidt, Prof. Dr. K. Betzler, Prof. Dr. M. Wöhlecke, Prof. Dr. M. Fally, brought interesting and important insight into various areas of physics.

My particular thanks to Prof. Dr. K. Bärwinkel and Prof. Dr. J. Schnack for providing me with useful experience while assisting a bit on their teaching activities.

Involving and diverse discussions with Prof. M. Shamonin, PD Dr. A. Postnikov, Dr. O. Zhuromskyy, Dr. J. Schnack, Dr. E. Shamonina, Prof. B. Sturman, I recall with high spirits.

Many thanks to the members of the working group, Dr. Maxim Gorkunov and Oleg Filippov, to all my colleagues, for nice and friendly atmosphere.

A vital role of financial support from the Deutsche Forschungsgemeinschaft enabled me to work within the Graduate College 695.

The last, but not least — many, many special thanks to Oleksandr Zhuromskyy and Tatjana Alekhina-Zhuromskaya, for their support and help; to Boris Feniouk and Zoia Tokmakova, for their playing a cardinal role for my appearing and remaining in Osnabrück; to all my friends, who also brightened and inspired my life these years and who are not to be mentioned here for the seek of maintaining privacy and security.

Eidesstattliche Erklärung

Hiermit erkläre ich an Eides Statt, die vorliegende Abhandlung selbständig und ohne unerlaubte Hilfe verfaßt, die benutzten Hilfsmittel vollständig angegeben und noch keinen Promotionsversuch unternommen zu haben.

Osnabrück, den 1. Juli 2004

(M. Lapine)

Tag der Einreichung:	1. Juli 2004
Tag der mündlichen Prüfung:	15. Juli 2004